Science Advances
AAAS

# Supplementary Materials for

## Free-electron Brewster-transition radiation

Ruoxi Chen *et al.*

Corresponding author: Xiao Lin, xiaolinzju@zju.edu.cn; Ido Kaminer, kaminer@technion.ac.il; Hongsheng Chen, hansomchen@zju.edu.cn

*Sci. Adv.* **9**, eadh8098 (2023)
DOI: 10.1126/sciadv.adh8098

**This PDF file includes:**

## Supplementary Methods

### Section S1: Free-electron transition radiation from a single interface

We begin with the analysis of free-electron transition radiation from a single interface, by following Ginzburg and Frank's theory of free-electron transition radiation (18,46,60-62,77). The interface is between region $j$ and region $j+1$ in Fig. S1, where $j$ is a positive integer. Both regions are composed of isotropic materials, whose relative permittivity are $\varepsilon_{\mathrm{r,j}}$ and $\varepsilon_{\mathrm{r,j+1}}$, respectively. The interface is at $z = z_{\mathrm{j}}$ and parallel to the $x$-$y$ plane. The moving electron has a charge of $q$ and a velocity of $\bar{v} = \hat{z}v$.

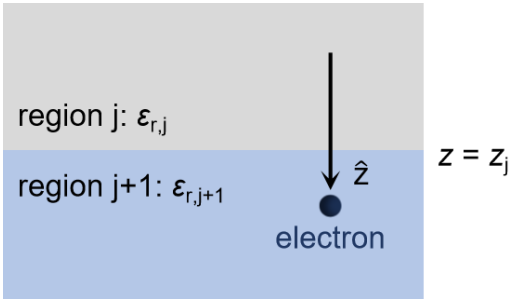


**Fig. S1. Schematic of free-electron transition radiation from a single interface.** Without loss of generality, the interface is set to be at $z = z_{\mathrm{j}}$.

From the Maxwell equations, we have

$$\nabla \times \bar{H}(\bar{r},t) = \bar{J}(\bar{r},t) + \varepsilon_0\varepsilon_{\mathrm{r}}\frac{\partial}{\partial t}\bar{E}(\bar{r},t) \tag{S1}$$

$$\nabla \times \bar{E}(\bar{r},t) = -\mu_0\mu_{\mathrm{r}}\frac{\partial}{\partial t}\bar{H}(\bar{r},t) \tag{S2}$$

where $\varepsilon_0$ and $\mu_0$ is the permittivity and the permeability of free space, respectively. The induced current density from the moving electron in equation (S1) is

$$\bar{J}(\bar{r},t) = \hat{z}qv\delta(x)\delta(y)\delta(z-vt) \tag{S3}$$

By applying the Fourier transformation, equation (S3) becomes to

$$\bar{J}(\bar{r},t) = \hat{z}J_{\mathrm{z}}^{q}(\bar{r},t) = \hat{z}\int d\omega \iint d\bar{k}_{\perp}\, j_{\bar{k}_{\perp},\omega}^{q}(z)e^{i\bar{k}_{\perp}\cdot\bar{r}_{\perp}}e^{-i\omega t} \tag{S4}$$

where $\bar{r}_\perp = \hat{x}x + \hat{y}y$ and $\bar{k}_\perp = \hat{x}k_\mathrm{x} + \hat{y}k_\mathrm{y}$. By combining equations (S3-S4), we have

$$j^q_{\bar{k}_\perp,\omega}(z) = \frac{q}{(2\pi)^3} e^{i\frac{\omega}{v}z} \tag{S5}$$

Similarly, by applying the Fourier transformation to the electric field $\bar{E}(\bar{r},t)$ and the magnetic field $\bar{H}(\bar{r},t)$ in equations (S1-S2), we have

$$\bar{E}(\bar{r},t) = \int d\omega \iint d\bar{k}_\perp \bar{E}_{\bar{k}_\perp,\omega}(z) e^{i\bar{k}_\perp\cdot\bar{r}_\perp} e^{-i\omega t} \tag{S6}$$

$$\bar{H}(\bar{r},t) = \int d\omega \iint d\bar{k}_\perp \bar{H}_{\bar{k}_\perp,\omega}(z) e^{i\bar{k}_\perp\cdot\bar{r}_\perp} e^{-i\omega t} \tag{S7}$$

By substituting equations (S6-S7) into equations (S1-S2) and after some calculations, we have

$$\frac{\partial^2}{\partial z^2}(\varepsilon_\mathrm{r}(z)E_\mathrm{z}(z)) + \left(\frac{\omega^2}{c^2}\varepsilon_\mathrm{r}(z) - k_\perp^2\right)\varepsilon_\mathrm{r}(z)E_\mathrm{z}(z) = -\frac{i\omega\mu_0 q}{(2\pi)^3}\left(\varepsilon_\mathrm{r}(z) - \frac{k_\perp^2 c^2}{v^2}\right)e^{i\frac{\omega}{v}z} \tag{S8}$$

where $E_\mathrm{z}(z)$ is the $z$ component of the electric field $\bar{E}_{\bar{k}_\perp,\omega}(z)$; $\varepsilon_\mathrm{r}$ is the relative permittivity, and we have $\varepsilon_\mathrm{r}(z) = \begin{cases}\varepsilon_{\mathrm{r,j}}; & \text{if } z < z_\mathrm{j} \\ \varepsilon_{\mathrm{r,j+1}}; & \text{if } z > z_\mathrm{j}\end{cases}$ according to Fig. S1.

The solution of $E_\mathrm{z}(z)$ in equation (S8) can be expressed as

$$E_\mathrm{z}(z) = E_\mathrm{z}^q(z) + E_\mathrm{z}^R(z) \tag{S9}$$

where $E_\mathrm{z}^q(z)$ corresponds to the charge field induced by the motion of electrons inside a homogeneous medium, and $E_\mathrm{z}^R(z)$ corresponds to the radiation field created by the electron's penetration through the interface. To be specific, in region $j$, we have

$$E^q_{\mathrm{z,j}}(z) = \frac{-iq}{\omega\varepsilon_0(2\pi)^3}\frac{1-\frac{c^2}{\varepsilon_{\mathrm{r,j}}v^2}}{\left(\varepsilon_{\mathrm{r,j}}-\frac{c^2}{v^2}-\frac{k_\perp^2c^2}{\omega^2}\right)}e^{i\frac{\omega}{v}z} \tag{S10}$$

$$E^{R,-}_{\mathrm{z,j}}(z) = \frac{iq}{\omega\varepsilon_0(2\pi)^3}a^{z=z_\mathrm{j},-}_{\mathrm{j,j+1}}e^{-ik_{\mathrm{z,j}}z} \tag{S11}$$

where $c = 1/\sqrt{\varepsilon_0\mu_0}$ is the speed of light in free space. Similarly, in region $j+1$, we have

$$E^q_{\mathrm{z,j+1}}(z) = \frac{-iq}{\omega\varepsilon_0(2\pi)^3}\frac{1-\frac{c^2}{\varepsilon_{\mathrm{r,j+1}}v^2}}{\left(\varepsilon_{\mathrm{r,j+1}}-\frac{c^2}{v^2}-\frac{k_\perp^2c^2}{\omega^2}\right)}e^{i\frac{\omega}{v}z} \tag{S12}$$

$$E^{R,+}_{\mathrm{z,j+1}}(z) = \frac{iq}{\omega\varepsilon_0(2\pi)^3}a^{z=z_\mathrm{j},+}_{\mathrm{j,j+1}}e^{ik_{\mathrm{z,j+1}}z} \tag{S13}$$

In equations (S10-S13), $k_{\mathrm{z,j}} = \sqrt{\frac{\omega^2}{c^2}\varepsilon_{\mathrm{r,j}} - k_\perp^2}$ is the $z$ component of wavevector in region $j$, and

$a_{\mathrm{j,j+1}}^{z=z_{\mathrm{j}},\pm}$ is the coefficient for radiation fields, where '$+$' ('$-$') stands for the excited waves propagating to the $+z$ $(-z)$ direction.

To obtain the rigorous expression for these radiation coefficients, the boundary conditions should be used, namely

$$\hat{n}\times\left(\bar{E}_{\mathrm{j}}-\bar{E}_{\mathrm{j+1}}\right)|_{z=z_{\mathrm{j}}}=0 \tag{S14}$$

$$\hat{n}\times\left(\bar{H}_{\mathrm{j}}-\bar{H}_{\mathrm{j+1}}\right)|_{z=z_{\mathrm{j}}}=0 \tag{S15}$$

where $\hat{n}=-\hat{z}$. By enforcing these boundary conditions, we have

$$a_{\mathrm{j,j+1}}^{z=z_{\mathrm{j}},-}=a_{\mathrm{j,j+1}}^{0,-}e^{+ik_{\mathrm{z,j}}z_{\mathrm{j}}}e^{i\frac{\omega}{v}z_{\mathrm{j}}} \tag{S16}$$

$$a_{j,j+1}^{z=z_{\mathrm{j}},+}=a_{\mathrm{j,j+1}}^{0,+}e^{-ik_{\mathrm{z,j+1}}z_{\mathrm{j}}}e^{i\frac{\omega}{v}z_{\mathrm{j}}} \tag{S17}$$

where

$$a_{\mathrm{j,j+1}}^{0,-}=\frac{\frac{v}{c}\frac{k_{\perp}^{2}c^{2}}{\omega^{2}\varepsilon_{\mathrm{r,j}}}\left(\varepsilon_{\mathrm{r,j+1}}-\varepsilon_{\mathrm{r,j}}\right)\left(1-\frac{v^{2}}{c^{2}}\varepsilon_{\mathrm{r,j}}+\frac{v}{c}\frac{k_{\mathrm{z,j+1}}}{\omega/c}\right)}{\left(1-\frac{v^{2}}{c^{2}}\varepsilon_{\mathrm{r,j}}+\frac{k_{\perp}^{2}v^{2}}{\omega^{2}}\right)\left(1+\frac{v}{c}\frac{k_{\mathrm{z,j+1}}}{\omega/c}\right)\left[\varepsilon_{\mathrm{r,j}}\frac{k_{\mathrm{z,j+1}}}{\omega/c}+\varepsilon_{\mathrm{r,j+1}}\frac{k_{\mathrm{z,j}}}{\omega/c}\right]} \tag{S18}$$

$$a_{\mathrm{j,j+1}}^{0,+}=\frac{\frac{v}{c}\frac{k_{\perp}^{2}c^{2}}{\omega^{2}\varepsilon_{\mathrm{r,j+1}}}\left(\varepsilon_{\mathrm{r,j+1}}-\varepsilon_{\mathrm{r,j}}\right)\left(1-\frac{v^{2}}{c^{2}}\varepsilon_{\mathrm{r,j+1}}-\frac{v}{c}\frac{k_{\mathrm{z,j}}}{\omega/c}\right)}{\left(1-\frac{v^{2}}{c^{2}}\varepsilon_{\mathrm{r,j+1}}+\frac{k_{\perp}^{2}v^{2}}{\omega^{2}}\right)\left(1-\frac{v}{c}\frac{k_{\mathrm{z,j}}}{\omega/c}\right)\left[\varepsilon_{\mathrm{r,j}}\frac{k_{\mathrm{z,j+1}}}{\omega/c}+\varepsilon_{\mathrm{r,j+1}}\frac{k_{\mathrm{z,j}}}{\omega/c}\right]} \tag{S19}$$

If $z_{\mathrm{j}}=0$ in Fig. S1, we actually have $a_{\mathrm{j,j+1}}^{z=z_{\mathrm{j}},\pm}=a_{\mathrm{j,j+1}}^{0,\pm}$.

## Section S2: Free-electron transition radiation from a slab

In this section, we derive the free-electron transition radiation from a slab. The slab has two parallel interfaces, which are at the plane of $z_1=0$ and $z_2=d$, respectively. As shown in Fig. S2, the electron perpendicularly penetrates through the slab with a thickness of $d$ and a relativity permittivity of $\varepsilon_{\mathrm{r},2}$.

The whole calculation procedure here is similar to that in section S1. After some calculations (18,46,60-62,77), one can obtain the total radiation field in each region, namely

$$E_{\mathrm{z},1}^{R}(z)=\frac{iq}{\omega\varepsilon_0(2\pi)^3}A_1^{-}e^{-ik_{\mathrm{z},1}z} \tag{S20}$$

$$E_{\mathrm{z},2}^{R}(z)=\frac{iq}{\omega\varepsilon_0(2\pi)^3}\left[A_2^{-}e^{-ik_{\mathrm{z},2}z}+A_2^{+}e^{ik_{\mathrm{z},2}z}\right] \tag{S21}$$

$$E_{\mathrm{z},3}^{R}(z)=\frac{iq}{\omega\varepsilon_0(2\pi)^3}A_3^{+}e^{ik_{\mathrm{z},3}(z-d)} \tag{S22}$$

In equations (S20-S22), $A_{\mathrm{j}}^{\pm}$ is the radiation coefficient in region $j$, where '+' ('−') stands for the excited waves propagating to the $+z$ $(-z)$ direction. To be specific, we have

$$A_1^{-}=a_{1,2}^{0,-}+a_{1,2}^{0,+}\frac{R_{2,3}T_{2,1}}{1-R_{2,1}R_{2,3}e^{2ik_{\mathrm{z},2}d}}e^{2ik_{\mathrm{z},2}d}+a_{2,3}^{0,-}\frac{T_{2,1}}{1-R_{2,1}R_{2,3}e^{e^{2ik_{\mathrm{z},2}d}}}e^{i\frac{\omega}{v}d}e^{ik_{\mathrm{z},2}d} \tag{S23}$$

$$A_2^{-}=a_{1,2}^{0,+}\frac{R_{2,3}}{1-R_{2,1}R_{2,3}e^{2ik_{\mathrm{z},2}d}}e^{2ik_{\mathrm{z},2}d}+a_{2,3}^{0,-}\frac{1}{1-R_{2,1}R_{2,3}e^{2ik_{\mathrm{z},2}d}}e^{i\frac{\omega}{v}d}e^{ik_{\mathrm{z},2}d} \tag{S24}$$

$$A_2^{+}=a_{1,2}^{0,+}\frac{1}{1-R_{2,1}R_{2,3}e^{2ik_{\mathrm{z},2}d}}+a_{2,3}^{0,-}\frac{R_{2,1}}{1-R_{2,1}R_{2,3}e^{2ik_{\mathrm{z},2}d}}e^{i\frac{\omega}{v}d}e^{ik_{\mathrm{z},2}d} \tag{S25}$$

$$A_3^{+}=a_{2,3}^{0,+}e^{i\frac{\omega}{v}d}+a_{1,2}^{0,+}\frac{T_{2,3}}{1-R_{2,1}R_{2,3}e^{2ik_{\mathrm{z},2}d}}e^{ik_{\mathrm{z},2}d}+a_{2,3}^{0,-}\frac{R_{2,1}T_{2,3}}{1-R_{2,1}R_{2,3}e^{2ik_{\mathrm{z},2}d}}e^{i\frac{\omega}{v}d}e^{2ik_{\mathrm{z},2}d} \tag{S26}$$

In equations (S23-S26), $R_{\mathrm{j,j+1}}$ and $R_{\mathrm{j+1,j}}$ ($T_{\mathrm{j,j+1}}$ and $T_{\mathrm{j+1,j}}$) correspond to the reflection (transmission) coefficients of *p*-polarized waves at the interface between region $j$ and $j+1$. Here all reflection and transmission coefficients are defined according to the electric field $E_{\mathrm{z}}$, that is,

$$R_{\mathrm{j,j+1}}=-R_{\mathrm{j+1,j}}=\frac{\varepsilon_{\mathrm{r,j+1}}k_{\mathrm{z,j}}-\varepsilon_{\mathrm{r,j}}k_{\mathrm{z,j+1}}}{\varepsilon_{\mathrm{r,j+1}}k_{\mathrm{z,j}}+\varepsilon_{\mathrm{r,j}}k_{\mathrm{z,j+1}}} \tag{S27}$$

$$T_{\mathrm{j,j+1}}=\frac{2\varepsilon_{\mathrm{r,j}}k_{\mathrm{z,j}}}{\varepsilon_{\mathrm{r,j+1}}k_{\mathrm{z,j}}+\varepsilon_{\mathrm{r,j}}k_{\mathrm{z,j+1}}} \tag{S28}$$

$$T_{\mathrm{j+1,j}}=\frac{\varepsilon_{\mathrm{r,j+1}}k_{\mathrm{z,j+1}}}{\varepsilon_{\mathrm{r,j+1}}k_{\mathrm{z,j}}+\varepsilon_{\mathrm{r,j}}k_{\mathrm{z,j+1}}} \tag{S29}$$

With the knowledge of the charge field and the radiation field in each region, the total field in equation (S9) in each region can be obtained. By exploiting the inverse Fourier transformation and after transforming the total field from the Cartesian coordinates $(x,y,z)$ into the cylindrical coordinates $(\rho,\phi,z)$ (18,46,60-62,77), we finally have

$$\begin{aligned}\bar{E}_{\mathrm{j}}^{q}(\bar{r},t)=\hat{z}\int_{-\infty}^{+\infty}d\omega\frac{-q}{8\pi\omega\varepsilon_0\varepsilon_{\mathrm{r,j}}}\left(\frac{\omega^2}{c^2}\varepsilon_{\mathrm{r,j}}-\frac{\omega^2}{v^2}\right)H_0^{(1)}\left(\rho\sqrt{\frac{\omega^2}{c^2}\varepsilon_{\mathrm{r,j}}-\frac{\omega^2}{v^2}}\right)e^{i\left(\frac{\omega}{v}z-\omega t\right)}+\\ \hat{\rho}\int_{-\infty}^{+\infty}d\omega\frac{-q}{8\pi\omega\varepsilon_0\varepsilon_{\mathrm{r,j}}}\left(i\frac{\omega}{v}\right)\left(-\sqrt{\frac{\omega^2}{c^2}\varepsilon_{\mathrm{r,j}}-\frac{\omega^2}{v^2}}\right)H_1^{(1)}\left(\rho\sqrt{\frac{\omega^2}{c^2}\varepsilon_{\mathrm{r,j}}-\frac{\omega^2}{v^2}}\right)e^{i\left(\frac{\omega}{v}z-\omega t\right)}\end{aligned} \tag{S30}$$

$$\bar{E}_{\mathrm{j}}^{R,-}(\bar{r},t)=\hat{z}\int_{-\infty}^{+\infty}d\omega\int_{0}^{+\infty}dk_{\perp}\frac{iq}{\omega\varepsilon_0(2\pi)^3}A_{\mathrm{j}}^{-}k_{\perp}\left(2\pi J_0(k_{\perp}\rho)\right)e^{i(-k_{\mathrm{z,j}}z-i\omega t)}+$$

$$\hat{\rho}\int_{-\infty}^{+\infty}d\omega\int_{0}^{+\infty}dk_{\perp}\frac{iq}{\omega\varepsilon_0(2\pi)^3}A_{\mathrm{j}}^{-}k_{\mathrm{z,j}}\left(i2\pi J_1(k_{\perp}\rho)\right)e^{i(-k_{\mathrm{z,j}}z-i\omega t)} \tag{S31}$$

$$\vec{E}_{\mathrm{j}}^{R,+}(\bar{r},t)=\hat{z}\int_{-\infty}^{+\infty}d\omega\int_{0}^{+\infty}dk_{\perp}\frac{iq}{\omega\varepsilon_0(2\pi)^3}A_{\mathrm{j}}^{+}k_{\perp}\left(2\pi J_0(k_{\perp}\rho)\right)e^{i(k_{\mathrm{z,j}}z-\omega t)}+$$

$$\hat{\rho}\int_{-\infty}^{+\infty}d\omega\int_{0}^{+\infty}dk_{\perp}\frac{iq}{\omega\varepsilon_0(2\pi)^3}A_{\mathrm{j}}^{+}\left(-k_{\mathrm{z,j}}\right)\left(i2\pi J_1(k_{\perp}\rho)\right)e^{i(k_{\mathrm{z,j}}z-\omega t)} \tag{S32}$$

*More information for equation (2) in the main text*

In the main text, we set

$$A_{\mathrm{forward}}=A_3^{+} \tag{S33}$$

$$a_{2,3}^{+}=a_{2,3}^{0,+}e^{i\frac{\omega}{v}d} \tag{S34}$$

$$a_{1,2}^{+}=a_{1,2}^{0,+}T_{2,3} \tag{S35}$$

$$a_{2,3}^{-}=a_{2,3}^{0,-}T_{2,3}e^{i\frac{\omega}{v}d} \tag{S36}$$

Then equation (S26) can be re-expressed as

$$A_{\mathrm{forward}}=a_{2,3}^{+}+a_{1,2}^{+}\frac{e^{ik_{\mathrm{z},2}d}}{1-R_{2,1}R_{2,3}e^{2ik_{\mathrm{z},2}d}}+a_{2,3}^{-}\frac{R_{2,1}e^{2ik_{\mathrm{z},2}d}}{1-R_{2,1}R_{2,3}e^{2ik_{\mathrm{z},2}d}} \tag{S37}$$

Equation (S37) exactly corresponds to equation (2) in the main text.

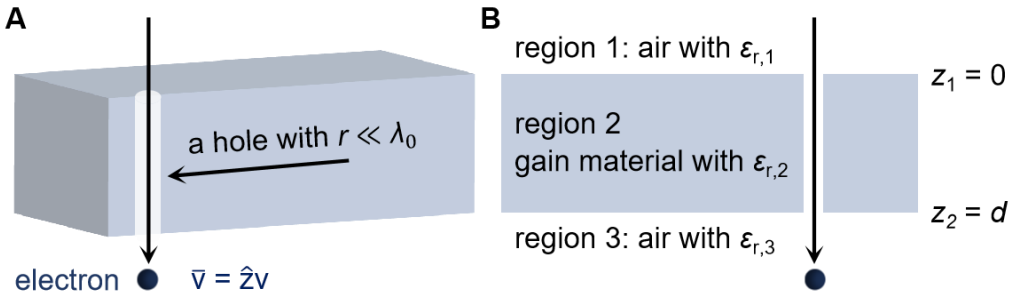


**Fig. S2. Structural schematic when a moving electron perpendicularly penetrates through a slab.** (**A**) 3D structural schematic. (**B**) 2D structural schematic. To avoid the potential inelastic scattering of swift electrons, a hole could be drilled for the slab; see Ref. (75,76) for example. The electron trajectory is along the hole's central line; and the hole's radius $r$ is much smaller than the working wavelength $\lambda_0$, namely $r \ll \lambda_0$.

*Free-electron Brewster-transition radiation from relativistic electrons*

The small hole along electron's trajectory is actually not mandatory for the creation of free-electron Brewster-transition radiation revealed in this work. For example, the highly-relativistic electrons themselves (e.g. $v/c > 0.95$) can safely penetrate through the gain slab with negligible inelastic electron scattering, and they can also enable the emergence of free-electron Brewster-transition radiation as shown in Fig. S3.

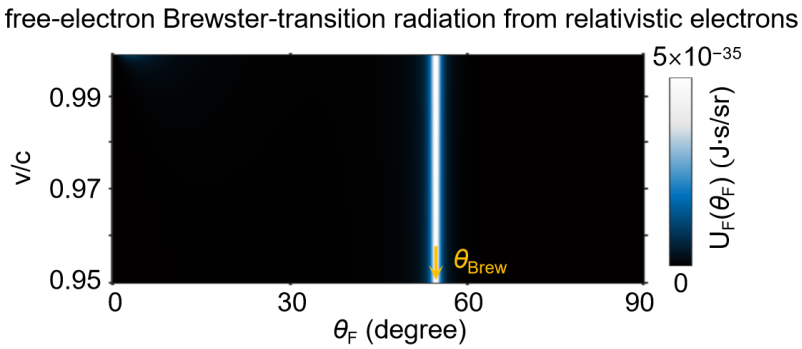


**Fig. S3 Free-electron Brewster-transition radiation from relativistic electrons (e.g. $v/c > 0.95$).** For illustration, here we plot the forward angular spectral energy density $U_{\mathrm{F}}(\theta_{\mathrm{F}})$ as a function of the electron velocity and the radiation angle. The structural setup here is the same as Fig. 1C, except for the range of electron velocity.

## Section S3: Comparison between $|a_{2,3}^{+}|$ and $|a_{2,3}^{-}|$ in equation (3)

This section serves as the complementary information for equations (3-4) in the main text. The definition of $a_{2,3}^{+}$ and $a_{2,3}^{-}$ are given in equations (S34&S36), respectively. According to their definitions, we show in Fig. S4 that $|a_{2,3}^{+}|$ and $|a_{2,3}^{-}|$ in equation (3) are in the same order of magnitude. This way, we could have $\left|a_{2,3}^{-}\frac{1}{R_{2,3}}\right| \gg |a_{2,3}^{+}|$ if $|R_{2,3}| \to 0$, which can be achieved if the radiation angle is close to the Brewster angle $\theta_{\mathrm{Brew}}$ (see the detailed discussion in section S6).

Then in the main text, it is feasible to further reduce equation (3) to equation (4).

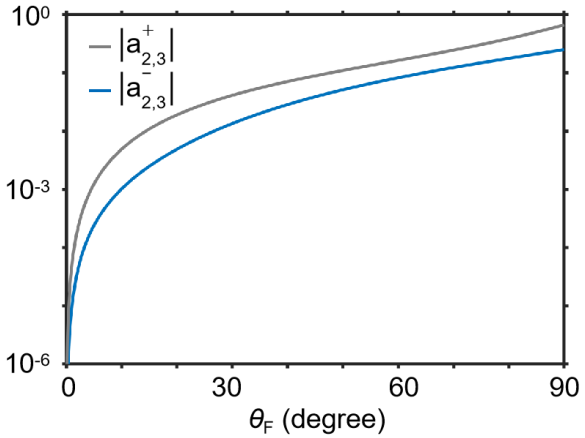


**Fig. S4. Dependence of $|a_{2,3}^{-}|$ and $|a_{2,3}^{+}|$ on the forward radiation angle $\theta_{\mathrm{F}}$.** This figure serves as the complementary information for equations (3-4) in the main text.

## Section S4: Angular spectral energy density of forward free-electron transition radiation

This section aims to calculate the angular spectral energy density of forward free-electron transition radiation (18,46,60-62,77). One can obtain the total radiated energy $W_{\mathrm{forward}}$ into the forward air region (namely region 3 in Fig. S2) by integrating the emitted field energy density over all space. For a long-enough time, the radiation field is already at the far field and well-separated from the charge field. If the origin is moved along the $z$-axis into the region of the radiated wave-train, the integration with respect to $z$ can be taken from $-\infty$ to $+\infty$, since the radiation field is attenuated in both directions. For freely propagating waves, the electric and magnetic energy densities are equal in free space, and one has

$$W_{\mathrm{forward}} = \iint dxdy \int_{-\infty}^{+\infty} dz \cdot \varepsilon_{\mathrm{r},3} \left|\bar{E}^{R}_{\mathrm{forward}}(\bar{r},t)\right|^2 \tag{S38}$$

where $\bar{E}^{R}_{\mathrm{forward}}(\bar{r},t) = \bar{E}^{R}_{3}(\bar{r},t)$, and we have

$$|\bar{E}^{R}_{3}(\bar{r},t)|^2 = \int d\omega d\omega' \iint d\bar{k}_{\perp} d\bar{k}'_{\perp}\, \bar{E}^{R}_{\bar{k}_{\perp},\omega,3}(\mathrm{z}) \cdot \left[\bar{E}^{R}_{\bar{k}'_{\perp},\omega',3}(\mathrm{z})\right]^{*} e^{i[(\bar{k}_{\perp}-\bar{k}'_{\perp})\cdot\bar{r}_{\perp}-(\omega-\omega')t]} \tag{S39}$$

By integrating over $dxdydzd\bar{k}'_{\perp}\, d\omega'$, equation (S38) reduces to

$$W_{\text{forward}} = 2\int_0^{+\infty} d\omega (2\pi)^3 \varepsilon_0 \varepsilon_{\text{r},3} \iint d\bar{k}_\perp \left[\frac{q}{\omega\varepsilon_0(2\pi)^3}\right]^2 |A_{\text{forward}}|^2 \frac{\omega^2}{ck_\perp^2}\sqrt{\varepsilon_{\text{r},3} - \frac{c^2k_\perp^2}{\omega^2}} \quad \text{(S40)}$$

For propagating waves, $\bar{k}_3 = \bar{k}_\perp + \hat{z}k_{\text{z},3}$ is the wavevector of radiation field in region 3, and we always have $k_\perp^2 \le k_3^2$, where $k_\perp = |\bar{k}_\perp|$ and $k_3 = \sqrt{\varepsilon_{\text{r},3}}\omega/c$. Since $\theta_{\text{F}}$ is the angle between $\bar{k}_3$ and $\bar{v}$, we actually have $k_\perp = \frac{\omega}{c}\sqrt{\varepsilon_{\text{r},3}}\sin\theta_{\text{F}}$. By changing the integration over $d\bar{k}_\perp$ in equation (S40) to the integration over $2\pi k_\perp dk_\perp = 2\pi\frac{\omega^2}{c^2}\varepsilon_{\text{r},3}\sin\theta_{\text{F}}\cos\theta_{\text{F}}d\theta_{\text{F}}$, we further have

$$W_{\text{forward}} = \int_0^{+\infty} d\omega \int_0^{\pi/2} U_{\text{forward}}(\theta_{\text{F}}, \omega)\cdot(2\pi\sin\theta_{\text{F}})d\theta_{\text{F}} \quad \text{(S41)}$$

where the forward angular spectral energy density $U_{\text{forward}}(\theta_{\text{F}}, \omega)$ is

$$U_{\text{forward}}(\theta_{\text{F}}, \omega) = \frac{\varepsilon_{\text{r},3}^{3/2} q^2 \cos^2\theta_{\text{F}}}{4\pi^3\varepsilon_0 c\sin^2\theta_{\text{F}}}|A_{\text{forward}}|^2 \quad \text{(S42)}$$

The forward angular spectral energy density in equation (S42) shows the dependence of the radiation intensity as a function of the forward radiation angle. For brevity, we use $U_{\text{F}}(\theta_{\text{F}}) = U_{\text{forward}}(\theta_{\text{F}}, \omega)$ in the main text.

## Section S5: Influence of the electron velocity on free-electron Brewster-transition radiation

This section serves the complementary information for Figs. 1C&4 in the main text. Here we show the forward angular spectral energy density $U_{\text{F}}(\theta_{\text{F}})$ of free-electron Brewster-transition radiation under different electron velocities in Fig. S5. Figure S5 shows that the ultrahigh directionality of free-electron Brewster-transition radiation shows up always at the Brewster angle. Moreover, the intensity of free-electron Brewster-transition radiation from a gain slab is four orders of magnitude larger than that of conventional free-electron transition radiation from a transparent slab. This large enhancement could occur at any electron velocity, even when $v/c \ll 1$, such as $v/c < 10^{-4}$ in Fig. S5A.

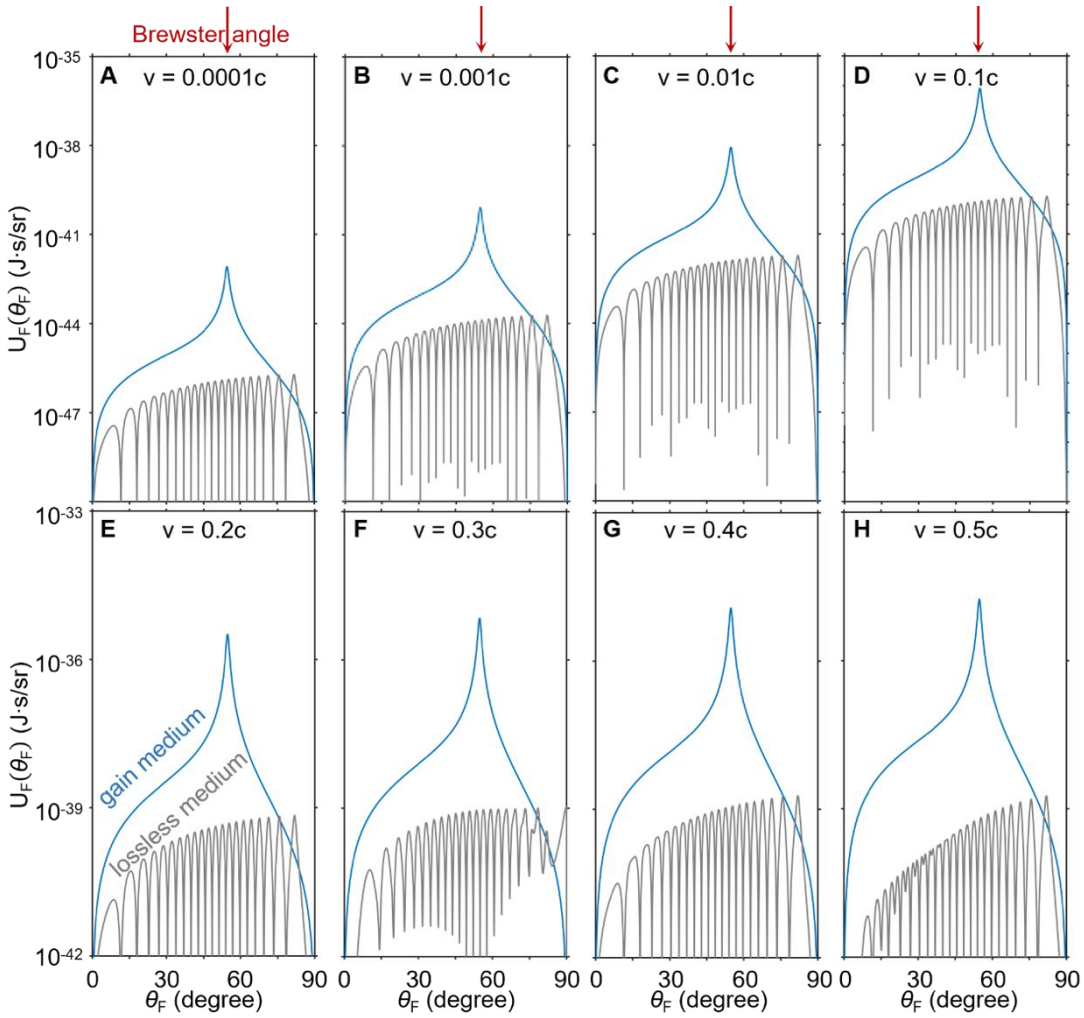


**Fig. S5. Forward angular spectral energy density of free-electron Brewster-transition radiation under different electron velocities.** For comparison, the forward angular spectral energy density of conventional free-electron transition radiation from a transparent slab is also given. The structural setup here is the same as Fig. 1C, except for the electron velocity. This figure serves as the complementary information for Fig. 1C&4.

## Section S6: Insensitivity of the pseudo-Brewster angle on the optical gain/loss

This section discusses the pseudo-Brewster effect in nonmagnetic systems with an optical loss or gain, and it serves as the complementary information for equations (3-4) in the main text. Historically, the Brewster effect is discovered in 1815 by the Scottish physicist Sir David Brewster

in a nonmagnetic and transparent system (78). The Brewster effect in nonmagnetic systems (64,78-80) corresponds to the phenomenon that the TM (or *p*-polarized) light is perfectly transmitted through an interface – then the reflection is zero, namely $R_{\mathrm{TM}} = 0$ – under a specific incident angle, which is widely known as the Brewster angle. Generally, $R_{\mathrm{TM}} = 0$ can only happen in transparent systems. If the system has a certain loss or gain, we cannot rigorously obtain $R_{\mathrm{TM}} = 0$. But a minimum of $|R_{\mathrm{TM}}|$ with $|R_{\mathrm{TM}}| \to 0$ is still achievable at a specific angle. Below $R_{2,3}$ is adopted as an example in Fig. S6. Figure S6 shows that this specific angle is relatively-insensitive to the optical gain or loss, and moreover, it is very close to the Brewster angle in the transparent system. Accordingly, this specific angle is denoted as the pseudo-Brewster angle, and the related phenomenon is denoted as the pseudo-Brewster effect according to previous works (52-59). Mathematically, the pseudo-Brewster angle for gain systems has $\theta_{\mathrm{Brew,pseudo}} = Re\left(\arctan\left(\sqrt{\varepsilon_{\mathrm{r},2}/\varepsilon_{\mathrm{r},3}}\right)\right)$, while the Brewster angle for transparent systems has $\theta_{\mathrm{Brew}} = \arctan\left(\sqrt{Re(\varepsilon_{\mathrm{r},2})/\varepsilon_{\mathrm{r},3}}\right)$. From Fig. S6, we can conclude that if $Im\left(\varepsilon_{\mathrm{r},2}\right)$ is reasonably large, $Re\left(\arctan\left(\sqrt{\varepsilon_{\mathrm{r},2}/\varepsilon_{\mathrm{r},3}}\right)\right) = \arctan\left(\sqrt{Re(\varepsilon_{\mathrm{r},2})/\varepsilon_{\mathrm{r},3}}\right)$, and thus $\theta_{\mathrm{Brew,pseudo}} = \theta_{\mathrm{Brew}}$. Therefore, for all figures in the main text, only the value of $\theta_{\mathrm{Brew}}$ is given.

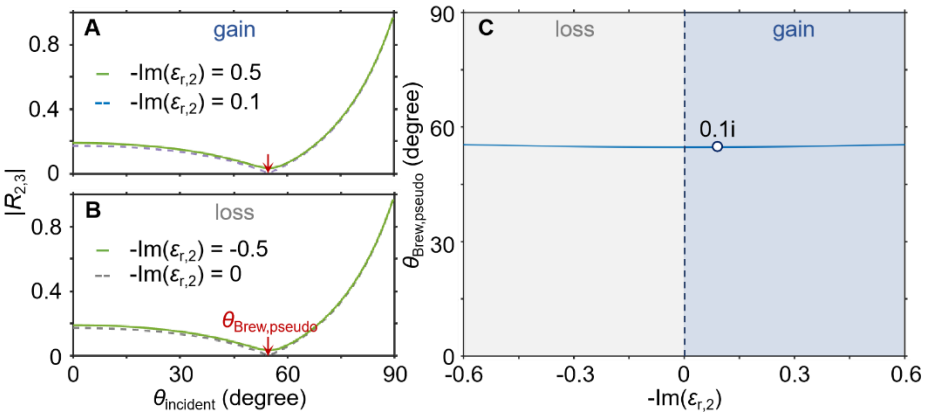


**Fig. S6. Dependence of the pseudo-Brewster angle $\theta_{\mathrm{Brew,pseudo}}$ on the value of $-Im(\varepsilon_{\mathrm{r},2})$.** (**A**), (**B**) Reflection of TM waves (e.g. $|R_{2,3}|$) as a function of the incident angle at different values

of $-Im(\varepsilon_{\mathrm{r},2})$. The minimum value of $|R_{2,3}|$ appears at the angle of $\theta_{\mathrm{Brew,pseudo}}$. (**C**) $\theta_{\mathrm{Brew,pseudo}}$ as a function of $-Im(\varepsilon_{\mathrm{r},2})$. If $\left|Im(\varepsilon_{\mathrm{r},2})\right|$ is reasonably large, we have $\theta_{\mathrm{Brew,pseudo}} = \theta_{\mathrm{Brew}}$, where $\theta_{\mathrm{Brew}}$ is the Brewster angle for transparent system. This figure serves as the complementary information for equations (3-4) in the main text.

## Section S7: Poles of the forward radiation coefficient $|A_{\mathrm{forward}}|$ on the complex $k_{\perp}$ plane

This section discusses the poles of $|A_{\mathrm{forward}}|$ on the complex $k_{\perp}$ plane and serves as the complementary information for Fig. 2. In this work, both regions 1 & 3 are free space, and region 2 is a dielectric material with a certain optical gain, as shown in Fig. S2. For conceptual demonstration, we let the electron velocity have $v < v_{\mathrm{th}}$ both inside and outside the slab so that there is no Cherenkov radiation in our studied system, where $v_{\mathrm{th}}$ is the Cherenkov threshold.

Upon close inspection of equation (2) in the main text (namely equation (S37)), the module of forward radiation coefficient $|A_{\mathrm{forward}}|$ from the dielectric systems considered in this work (namely $Re(\varepsilon_{\mathrm{r,j}}) > 0$) would become infinite, if

$$\frac{R_{2,1}e^{2ik_{\mathrm{z},2}d}}{1-R_{2,1}R_{2,3}e^{2ik_{\mathrm{z},2}d}} = \infty \tag{S43}$$

*Case 1: Transparent slab*

If the slab is lossless, region 2 in Fig. S2 is considered to have a relative permittivity of $Re(\varepsilon_{\mathrm{r},2})$. For this lossless case, since the value of $R_{2,1}e^{2ik_{\mathrm{z},2}d}$ is finite, the condition in equation (S43) actually corresponds to

$$\frac{1}{1-R_{2,1}R_{2,3}e^{2ik_{\mathrm{z},2}d}} = \infty \tag{S44}$$

which is exactly the guidance condition for a transparent slab (64). This way, all poles for $|A_{\text{forward}}|$ in the complex $k_\perp$ plane correspond to the guided modes supported by the transparent slab. In the complex $k_\perp$ plane, the value of $Re(k_\perp)$ for all guided modes is denoted as $k_{\perp,\text{guidance}}$. From the guidance condition, we have $k_{\text{air}} < k_{\perp,\text{guidance}} < Re(k_2)$ as shown in Fig. S7, where $Re(k_2) = \sqrt{Re(\varepsilon_{\text{r},2})}\omega/c$.

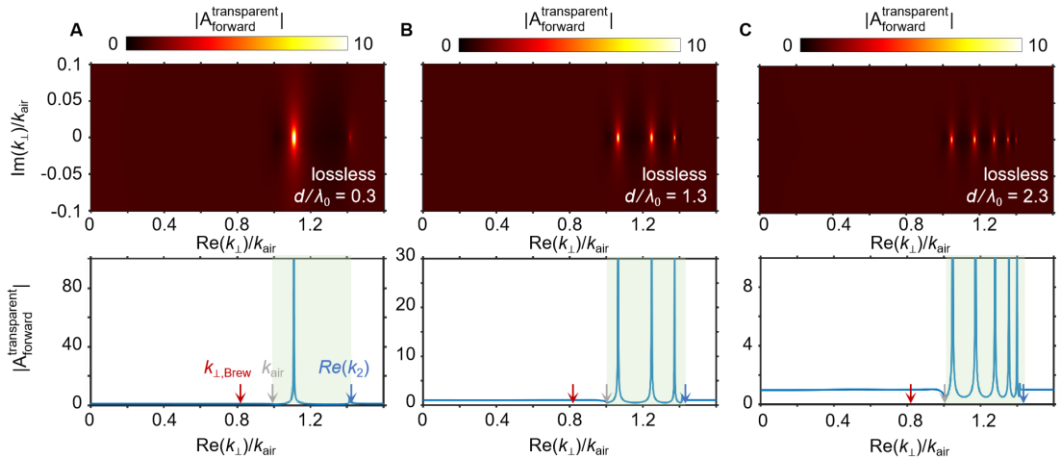


**Fig. S7. Poles of $|A_{\text{forward}}|$ in the complex $k_\perp$ plane, if the slab is transparent.** This figure serves as the complementary information for Fig. 2D. The transparent dielectric slab has a relative permittivity of $Re(\varepsilon_{\text{r},2})$. (**A**)-(**C**) Thickness influence on the poles of $|A_{\text{forward}}^{\text{transparent}}| = |\frac{1}{1-R_{2,1}R_{2,3}e^{2ik_{\text{z},2}d}}|$, according to equation (S44). The upper panels show the values of $|A_{\text{forward}}^{\text{transparent}}|$ in the complex $k_\perp$ plane. The bottom panels show the dependence of $|A_{\text{forward}}^{\text{transparent}}|$ on $Re(k_\perp)$ by setting $Im(k_\perp) = 0$. All the poles have $Re(k_2) > Re(k_\perp) = k_{\perp,\text{guidance}} > k_{\text{air}}$ and correspond to the guided modes supported by a transparent slab. This way, these poles would not contribute to the free-electron transition radiation into the far field.

*Case 2: Gain slab with a relatively-thin thickness*

For the gain slab, we consider the cases, here and below, that the optical gain is fixed with $-Im(\varepsilon_{\text{r},2}) = 0.1$, and we consider the slab thickness is relatively thin so that the free-electron

transition radiation is in the conventional or intermediate phases. Due to the existence of gain in the slab, we have $Im(k_{z,2}) < 0$ and thus $|e^{2ik_{z,2}d}| > 1$; moreover, since the thickness of the gain slab is relatively-thin, the value of $|e^{2ik_{z,2}d}|$ is finite. To fulfill the condition in equation (S43), $|R_{2,1}R_{2,3}|$ should be less than one, which in principle is possible in the complex $k_\perp$ plane. By plotting $|A^{\text{gain}}_{\text{forward}}| = |\frac{R_{2,1}e^{2ik_{z,2}d}}{1-R_{2,1}R_{2,3}e^{2ik_{z,2}d}}|$ in the complex $k_\perp$ plane, we find in Fig. S8 that all poles show up in the fourth quadrant (and the second quadrant, not shown in the figure) of the complex $k_\perp$ plane. If the slab thickness is very small (e.g. $d/\lambda_0 = 1.3$ in Fig. S8A), the poles appear only with $Re(k_2) > Re(k_\perp) > k_{\text{air}}$ and correspond to the guided modes, which are similar to the transparent case in Fig. S7 and would not contribute to the far-field radiation. When the slab thickness increases (e.g. $d/\lambda_0 = 5.3$ in Fig. S8B or $d/\lambda_0 = 13.3$ in Fig. S8C), a new type of poles appears with $Re(k_\perp) < k_{\text{air}}$, but the values of $Re(k_\perp)$ for these poles are sensitive to the slab thickness. Since $Re(k_\perp) < k_{\text{air}}$, these poles correspond to some leaky eigenmodes, which can contribute to the far-field radiation.

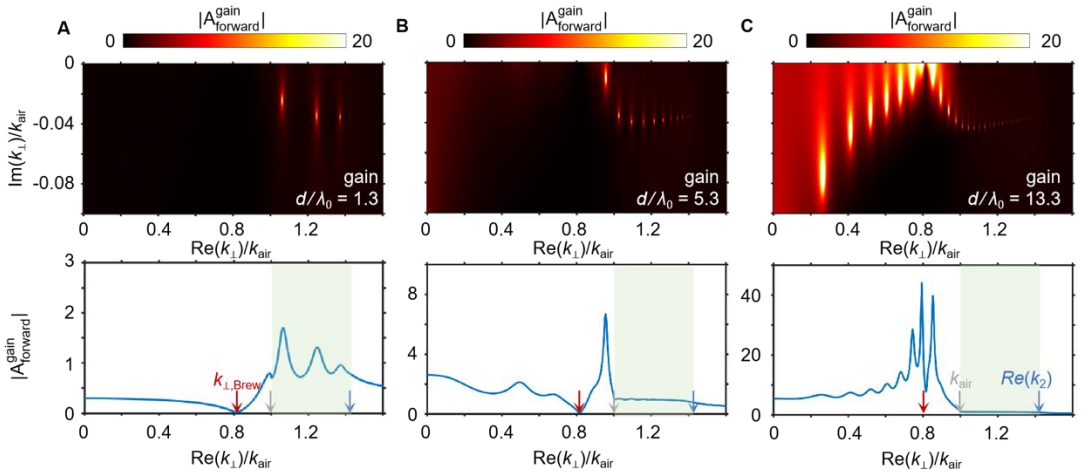


**Fig. S8. Poles of $|A_{\text{forward}}|$ in the complex $k_\perp$ plane, if the gain slab has a relatively-thin thickness.** This figure serves as the complementary information for Fig. 2. For the gain slab, its gain with $-Im(\varepsilon_{r,2}) = 0.1$ is used, and its thickness is relatively thin so that the free-electron transition

radiation is in the conventional or intermediate phase. (**A**)-(**C**) Thickness influence on the poles of $A_{\text{forward}}^{\text{gain}} = \frac{R_{2,3}e^{2ik_{z,2}d}}{1-R_{2,1}R_{2,3}e^{2ik_{z,2}d}}$, according to equation (S43). The upper panels show the values of $|A_{\text{forward}}^{\text{gain}}|$ in the complex $k_\perp$ plane. The bottom panels show the dependence of $|A_{\text{forward}}^{\text{gain}}|$ on $Re(k_\perp)$ by setting $Im(k_\perp) = 0$. There are two types of poles. One type of poles has $Re(k_2) > Re(k_\perp) > k_{\text{air}}$, which would not contribute to the far-field radiation. The other type of poles has $Re(k_\perp) < k_{\text{air}}$, which can contribute to the far-field radiation, but the value of $Re(k_\perp)$ is sensitive to the slab thickness.

*Case 3: Gain slab with an infinitely-large thickness*

Here we consider the gain slab with a large-enough thickness so that the free-electron transition radiation is in the Brewster phase. By plotting $|A_{\text{forward}}^{\text{gain}}| = |\frac{R_{2,1}e^{2ik_{z,2}d}}{1-R_{2,1}R_{2,3}e^{2ik_{z,2}d}}|$ in the complex $k_\perp$ plane, we find in Fig. S9 that all poles show up in the second or fourth quadrant of the complex $k_\perp$ plane. Actually, these poles can be categorized into three types. The first type of poles has $Re(k_2) > Re(k_\perp) > k_{\text{air}}$, and the second type of poles has $Re(k_\perp) < k_{\text{air}}$ with the value of $Re(k_\perp)$ being sensitive to the slab thickness. These two types in Fig. S9 are similar to the ones discussed in Fig. S8. The third type of poles is featured with $Re(k_\perp) = k_{\perp,\text{Brew}}$, and the value of $Re(k_\perp)$ is insensitive to the slab thickness, where $k_{\perp,\text{Brew}} = k_{\text{air}}sin\theta_{\text{Brew}} < k_{\text{air}}$. Actually, for the gain slab, if $d/\lambda_0 \to \infty$, since $\left|e^{2ik_{z,2}d}\right| \to \infty$ and $\left|R_{2,1}R_{2,3}e^{2ik_{z,2}d}\right| \gg 1$, equation (S43) can be reduced to

$$\lim_{d\to\infty} \frac{R_{2,1}e^{2ik_{z,2}d}}{1-R_{2,1}R_{2,3}e^{2ik_{z,2}d}} = -\frac{1}{R_{2,3}} \tag{S45}$$

This way, the pole of $|A_{\text{forward}}|$ or $|A_{\text{forward}}^{\text{gain}}|$ corresponds to the solution of $R_{2,3} = 0$. According to the pseudo-Brewster effect of gain materials, this solution has $|Re(k_\perp)| = k_{\perp,\text{Brew}}$; this way, the

third type of poles always appears with $|Re(k_\perp)| = k_{\perp,\mathrm{Brew}}$. Due to its close connection with the pseudo-Brewster effect of gain materials, the leaky eigenmode related to the third type of poles is termed as the Brewster leaky mode in Fig. 2C, which can be efficiently excited and contribute to the far-field radiation.

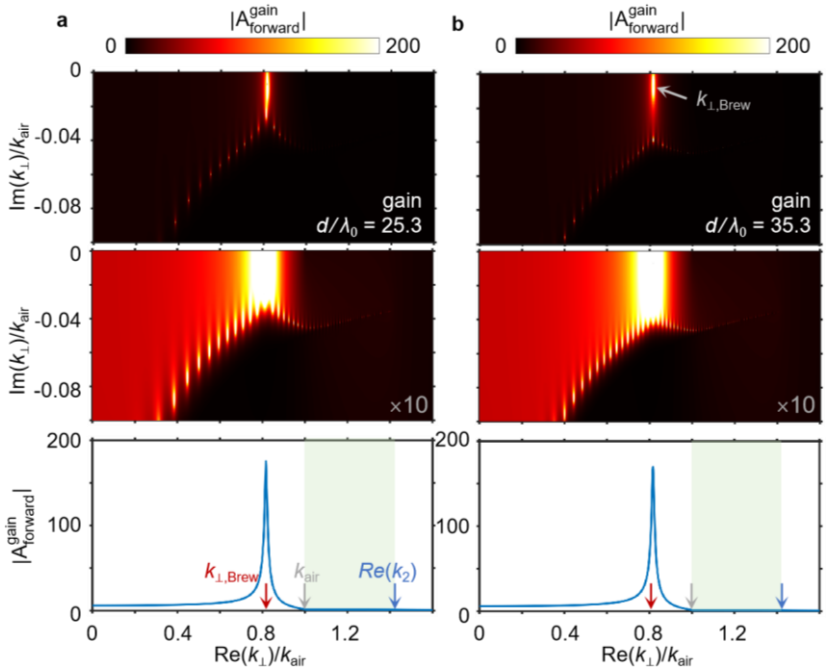


**Fig. S9. Poles of $|A_{\mathrm{forward}}|$ in the complex $k_\perp$ plane, if the gain slab has a large-enough thickness.** This figure serves as the complementary information for Fig. 2C. For the gain slab, its gain with $-Im(\varepsilon_{r,2}) = 0.1$ is used, and its thickness is large enough so that the free-electron transition radiation is in the Brewster phase. (**A**), (**B**) Thickness influence on the poles of $|A^{\mathrm{gain}}_{\mathrm{forward}}| = |\frac{R_{2,3}e^{2ik_{z,2}d}}{1-R_{2,1}R_{2,3}e^{2ik_{z,2}d}}|$, according to equation (S43). The upper panels show the values of $|A^{\mathrm{gain}}_{\mathrm{forward}}|$ in the complex $k_\perp$ plane. The bottom panels show the dependence of $|A^{\mathrm{gain}}_{\mathrm{forward}}|$ on $Re(k_\perp)$ by setting $Im(k_\perp) = 0$. There are three types of poles. One type of poles has $Re(k_2) > Re(k_\perp) > k_{\mathrm{air}}$, which would not contribute to the far-field radiation. The second type of poles has $Re(k_\perp) < k_{\mathrm{air}}$, but the value of $Re(k_\perp)$ is sensitive to the slab thickness. The third type of poles has $Re(k_\perp) = k_{\perp,\mathrm{Brew}}$, and the value of $Re(k_\perp)$ is insensitive to the slab thickness. From the

comparison of $|A_{\text{forward}}^{\text{gain}}|$ with $Im(k_\perp) = 0$ in Figs. S8-S9, the maximum value of $|A_{\text{forward}}^{\text{gain}}|$ for free-electron transition radiation in the Brewster phase in Fig. S9 is much larger than that of free-electron transition radiation in the conventional or intermediate phase in Fig. S8. This indicates that the Brewster leaky mode (which corresponds to the third type of poles) could be excited more efficiently than other leaky modes (which correspond to the second type of poles).

## Section S8: Dependence of the angular deviation $\Delta\theta$ on the slab thickness under different optical gains

This section serves as the complementary information for Fig. 3B-C and shows the dependence of the angular deviation $\Delta\theta$ on the slab thickness under various optical gains, where the definition of $\Delta\theta$ is given in Fig. 3A.

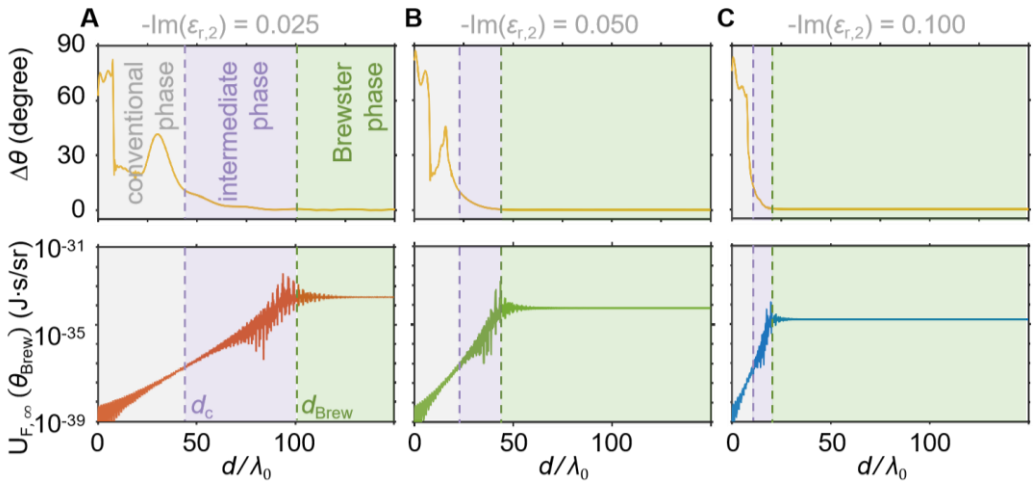


**Fig. S10. Dependence of the angular deviation $\Delta\theta$ on the slab thickness $d$ under different optical gains.** This serves as the complementary information for Fig. 3B-C. When the free-electron transition radiation is in the Brewster phase, we have $\Delta\theta < \Delta\theta_{\text{Brew}}$ and its radiation intensity is insensitive to the variation of the slab thickness, where $\Delta\theta_{\text{Brew}} = 0.5°$.

**Section S9: Forward angular spectral energy density of free-electron transition radiation from a lossy slab**

This section serves as the complementary information for Fig. 3C, and we show the forward angular spectral energy density of free-electron transition radiation from a lossy slab in Fig. S11.

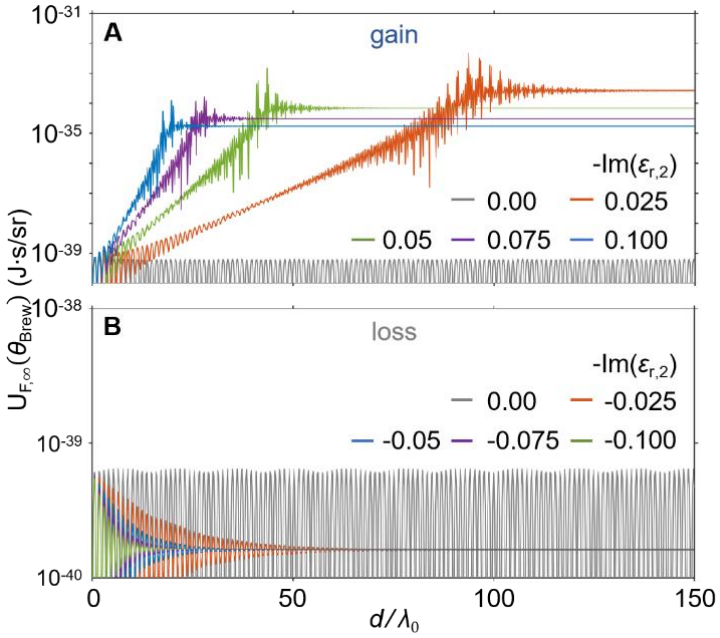


**Fig. S11. Forward angular spectral energy density of free-electron transition radiation from a lossy slab.** For comparison, the case from a gain slab is also added in this figure. (**A**) A slab with a certain optical gain. (**B**) A slab with a certain optical loss. The structural setup here is the same as that in Fig. 3C, except for the value of $-Im(\varepsilon_{r,2})$. This figure serves as the complementary information for Fig. 3C. When $d/\lambda_0$ is large enough in (B), the radiation intensity from a lossy slab becomes insensitive to the variation of the slab thickness, but its value is orders of magnitude smaller than that from a gain slab.

## Section S10: Influence of frequency dispersion and anisotropy on free-electron Brewster-transition radiation

*Influence of frequency dispersion on free-electron Brewster-transition radiation*

In practice, the gain medium is generally dispersive, such as Rhodamine 6G (R6G) with its relative permittivity shown in Fig. S12A. When considering the frequency dispersion, the revealed free-electron Brewster-transition radiation would always appear at the corresponding Brewster angle, whose value is frequency dependent; see Fig. S12B-C for example.

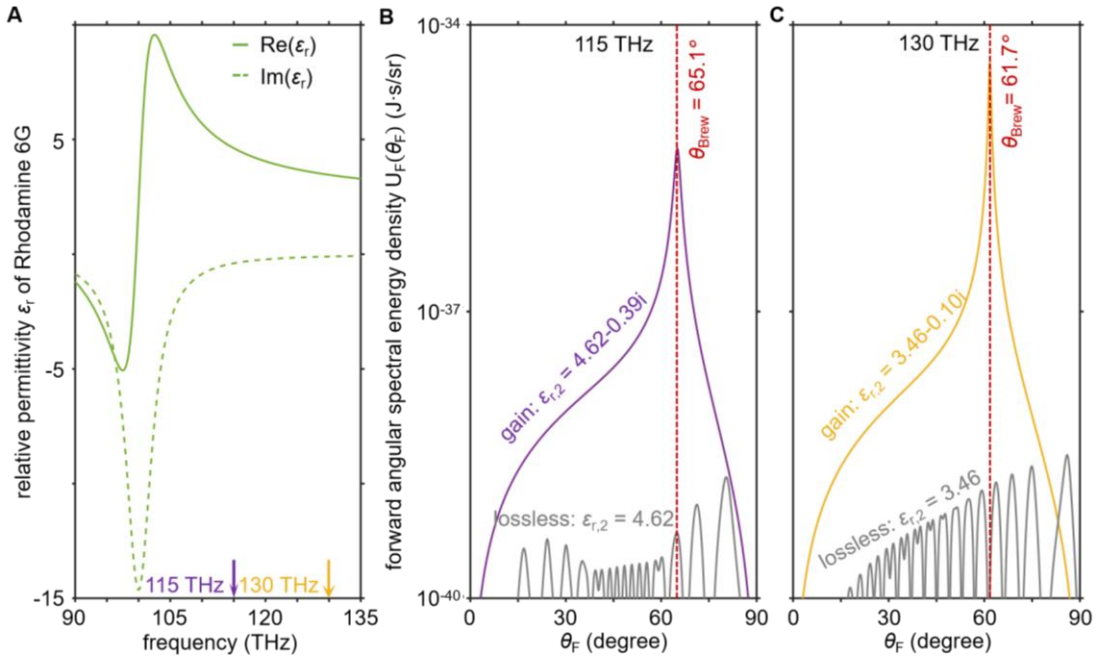


**Fig. S12. Free-electron Brewster-transition radiation under the consideration of frequency dispersion for the gain medium.** For illustration, here we use Rhodamine 6G (R6G) (72) as the gain medium. The other structural setup is the same as Fig. 1C. (**A**) Relative permittivity of R6G as a function of frequency, whose calculation is based on the four-level atomic model (72). The basic setup is the same as Ref. (72). That is, the total dye concentration is $N_0(t=0) = 5.0 \times 10^{23}$ m$^{-3}$, the lifetime $\tau_{l_m,l_n}$ for the transition from level $l_m$ to the lower level $l_n$ is $\tau_{3,2} = 5.0 \times 10^{-14}$ s, $\tau_{2,1} = 5.0 \times 10^{-12}$ s, and $\tau_{1,0} = 5.0 \times 10^{-14}$ s, the pumping rate from level 0 to level 3 is $\Gamma_{\text{pump}} =$

$4.7 \times 10^9\ \mathrm{s}^{-1}$, the center frequency of the radiation is $\omega_\mathrm{a}/2\pi = 10^{14}$ Hz, the coupling strength is $\sigma_\mathrm{a} = 10^{-4}\ \mathrm{C}^2/\mathrm{kg}$, and the linewidth of the atomic transition is $\Gamma_\mathrm{a}/2\pi = 5 \times 10^{12}$ Hz. (**B**), (**C**) Forward angular spectral energy density $U_\mathrm{F}(\theta_\mathrm{F})$ of free-electron radiation at different working frequencies. The working frequency is 115 THz in (B) and 130 THz in (C). To avoid the influence of Cherenkov radiation, the electron velocity is set to be $v/c = 0.4$. For comparison, the forward free-electron radiation from each corresponding lossless medium is also provided.

*Free-electron Brewster-transition radiation from gain materials with an experimentally-obtained permittivity*

We show in Fig. S13 the free-electron Brewster-transition radiation by using gain materials with an experimentally-obtained permittivity. According to the experimental work in Ref. [81], the measured relative permittivity of the gain material Rhodamine 6G (R6G) under certain optical pumping is $\varepsilon_\mathrm{R6G}(\lambda_0) = 2.25 - 0.006i$ at the working wavelength $\lambda_0 = 532$ nm. Accordingly, this relative permittivity is used in Fig. S13.

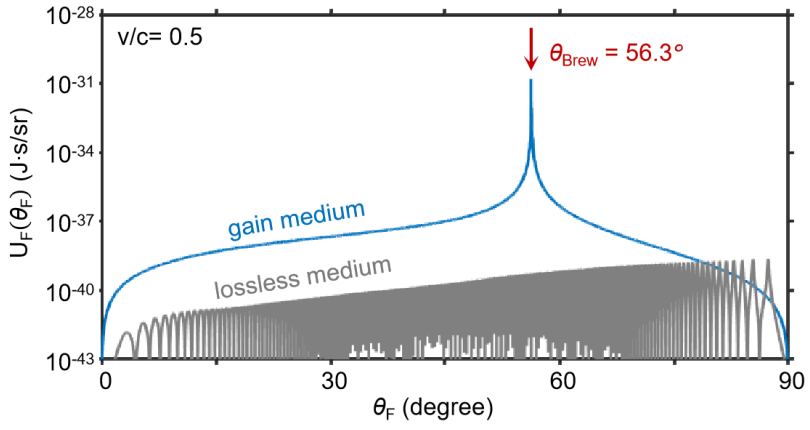


**Fig. S13. Free-electron Brewster-transition radiation from gain materials with an experimentally-obtained permittivity.** According to the experimental work of Ref. [81], the gain medium Rhodamine 6G (R6G) under certain optical pumping has a relative permittivity of

$\varepsilon_{\mathrm{r},2}(\lambda_0) = 2.25 - 0.006i$ at the working wavelength of $\lambda_0 = 532$ nm. This relative permittivity and the working wavelength are used in this plot. For illustration, the slab thickness is set to be $d = 500\lambda_0$, and the other structural setup is the same as Fig. 1C. Under this scenario, the phenomenon of free-electron Brewster-transition radiation would also emerge. For comparison, the forward free-electron radiation from the corresponding lossless medium is also provided.

*Influence of anisotropy on free-electron Brewster-transition radiation*

When region 2 is filled by a uniaxial material with a relative permittivity of $\bar{\bar{\varepsilon}}_{\mathrm{r},2} = [\varepsilon_{\perp,2}, \varepsilon_{\perp,2}, \varepsilon_{z,2}]$, the calculation procedure of free-electron radiation from a uniaxial system is similar to that from an isotropic medium (62). After some efforts, the radiation coefficients $a_{1,2}^{0,\pm}$ and $a_{2,3}^{0,\pm}$ in equation (S23-S26) should be changed to:

$$a_{1,2}^{0,-} = \frac{\kappa_\perp^2 c^2}{\omega^2} \cdot \frac{-v}{c} \cdot \varepsilon_{\perp,2} \frac{\frac{1-\frac{v}{c}\frac{k_{z,2}}{\omega/c}}{\varepsilon_{z,2}(1-\frac{v^2}{c^2}\varepsilon_{\perp,2}+\frac{\kappa_\perp^2 v^2}{\omega^2}\frac{\varepsilon_{\perp,2}}{\varepsilon_{z,2}})} - \frac{1-\frac{v}{c}\frac{k_{z,2}}{\omega/c}\frac{\varepsilon_{\mathrm{r},1}}{\varepsilon_{\perp,2}}}{\varepsilon_1(1-\frac{v^2}{c^2}\varepsilon_{\mathrm{r},1}+\frac{\kappa_\perp^2 v^2}{\omega^2})}}{\varepsilon_{\mathrm{r},1}\frac{k_{z,2}}{\omega/c}+\varepsilon_{\perp,2}\frac{k_{z,1}}{\omega/c}} \tag{S46}$$

$$a_{1,2}^{0,+} = \frac{\kappa_\perp^2 c^2}{\omega^2} \cdot \frac{+v}{c} \cdot \frac{\varepsilon_{\mathrm{r},1}\varepsilon_{\perp,2}}{\varepsilon_{z,2}} \frac{\frac{1+\frac{v}{c}\frac{k_{z,1}}{\omega/c}}{\varepsilon_{\mathrm{r},1}(1-\frac{v^2}{c^2}\varepsilon_{\mathrm{r},1}+\frac{\kappa_\perp^2 v^2}{\omega^2})} - \frac{1+\frac{v}{c}\frac{k_{z,1}}{\omega/c}\frac{\varepsilon_{\perp,2}}{\varepsilon_{\mathrm{r},1}}}{\varepsilon_{z,2}(1-\frac{v^2}{c^2}\varepsilon_{\perp,2}+\frac{\kappa_\perp^2 v^2}{\omega^2}\frac{\varepsilon_{\perp,2}}{\varepsilon_{z,2}})}}{\varepsilon_{\mathrm{r},1}\frac{k_{z,2}}{\omega/c}+\varepsilon_{\perp,2}\frac{k_{z,1}}{\omega/c}} \tag{S47}$$

$$a_{2,3}^{0,-} = \frac{\kappa_\perp^2 c^2}{\omega^2} \cdot \frac{-v}{c} \cdot \frac{\varepsilon_{\perp,2}\varepsilon_{\mathrm{r},3}}{\varepsilon_{z,2}} \frac{\frac{1-\frac{v}{c}\frac{k_{z,3}}{\omega/c}}{\varepsilon_{\mathrm{r},3}(1-\frac{v^2}{c^2}\varepsilon_{\mathrm{r},3}+\frac{\kappa_\perp^2 v^2}{\omega^2})} - \frac{1-\frac{v}{c}\frac{k_{z,3}}{\omega/c}\frac{\varepsilon_{\perp,2}}{\varepsilon_{\mathrm{r},3}}}{\varepsilon_{z,2}(1-\frac{v^2}{c^2}\varepsilon_{\perp,2}+\frac{\kappa_\perp^2 v^2}{\omega^2}\frac{\varepsilon_{\perp,2}}{\varepsilon_{z,2}})}}{\varepsilon_{\perp,2}\frac{k_{z,3}}{\omega/c}+\varepsilon_{\mathrm{r},3}\frac{k_{z,2}}{\omega/c}} \tag{S48}$$

$$a_{2,3}^{0,+} = \frac{\kappa_\perp^2 c^2}{\omega^2} \cdot \frac{+v}{c} \cdot \varepsilon_{\perp,2} \frac{\frac{1+\frac{v}{c}\frac{k_{z,2}}{\omega/c}}{\varepsilon_{z,2}(1-\frac{v^2}{c^2}\varepsilon_{\perp,2}+\frac{\kappa_\perp^2 v^2}{\omega^2}\frac{\varepsilon_{\perp,2}}{\varepsilon_{z,2}})} - \frac{1+\frac{v}{c}\frac{k_{z,2}}{\omega/c}\frac{\varepsilon_{\mathrm{r},3}}{\varepsilon_{\perp,2}}}{\varepsilon_{\mathrm{r},3}(1-\frac{v^2}{c^2}\varepsilon_{\mathrm{r},3}+\frac{\kappa_\perp^2 v^2}{\omega^2})}}{\varepsilon_{\perp,2}\frac{k_{z,3}}{\omega/c}+\varepsilon_{\mathrm{r},3}\frac{k_{z,2}}{\omega/c}} \tag{S49}$$

Accordingly, the reflection coefficients in equations (S23-S26) become to $R_{2,1} = \frac{\frac{k_{z,2}}{\varepsilon_{\perp,2}} - \frac{k_{z,1}}{\varepsilon_{\mathrm{r},1}}}{\frac{k_{z,2}}{\varepsilon_{\perp,2}} + \frac{k_{z,1}}{\varepsilon_{\mathrm{r},1}}}$ and

$R_{2,3} = \frac{\frac{k_{z,2}}{\varepsilon_{\perp,2}} - \frac{k_{z,3}}{\varepsilon_{r,3}}}{\frac{k_{z,2}}{\varepsilon_{\perp,2}} + \frac{k_{z,3}}{\varepsilon_{r,3}}}$. Similarly, the transmission coefficients in equations (S23-S26) become to $T_{2,1} = \frac{2\frac{k_{z,2}\varepsilon_{z,2}}{\varepsilon_{\perp,2}\varepsilon_{r,1}}}{\frac{k_{z,2}}{\varepsilon_{\perp,2}} + \frac{k_{z,1}}{\varepsilon_1}}$; $T_{2,3} = \frac{2\frac{k_{z,2}\varepsilon_{z,2}}{\varepsilon_\perp\ \varepsilon_{r,3}}}{\frac{k_{z,2}}{\varepsilon_{\perp,2}} + \frac{k_{z,3}}{\varepsilon_{r,3}}}$, where $k_{z,2} = \sqrt{\frac{\omega^2}{c^2}\varepsilon_{\perp,2} - \frac{\varepsilon_{\perp,2}}{\varepsilon_{z,2}}k_\perp^2}$. Moreover, the Brewster angle should now be expressed as $\theta_{\text{Brew}} = \arctan\left(Re\left(\sqrt{\frac{\varepsilon_{z,2}(\varepsilon_{\perp,2}-\varepsilon_{r,1})}{\varepsilon_{r,1}(\varepsilon_{z,2}-\varepsilon_{r,1})}}\right)\right)$.

When considering the gain medium with anisotropy, such as a uniaxial gain medium, we show in Fig. S14 that the revealed free-electron Brewster-transition radiation also exists.

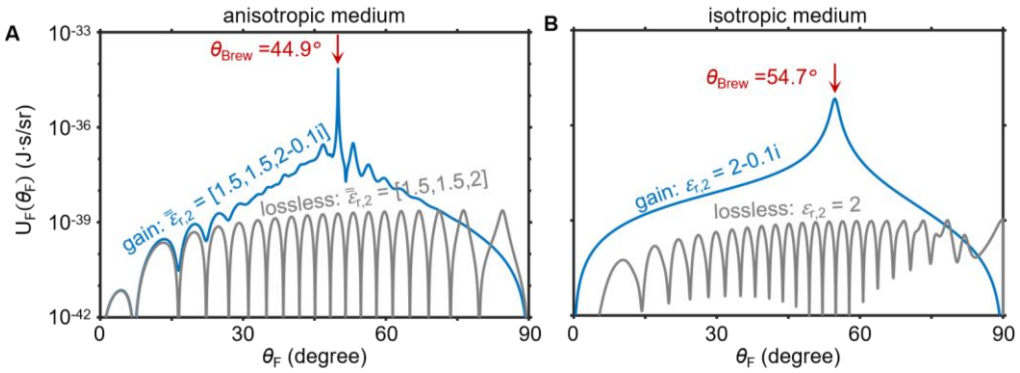


**Fig. S14. Free-electron Brewster-transition radiation from a gain uniaxial slab.** Here, we show the forward angular spectral energy density $U_{\text{F}}(\theta_{\text{F}})$ of free-electron transition radiation from a uniaxial slab. The structural setup is the same as Fig. 1, except for the relative permittivity. (**A**) A uniaxial slab with a relative permittivity of $\bar{\bar{\varepsilon}}_{\text{r},2} = [1.5,1.5,2 - 0.1i]$. (**B**) An isotropic medium with a relative permittivity of $\varepsilon_{\text{r},2} = 2 - 0.1i$. For comparison, the free-electron transition radiation from a lossless uniaxial ($\bar{\bar{\varepsilon}}_{\text{r},2} = [1.5,1.5,2]$) or isotropic ($\varepsilon_{\text{r},2} = 2$) medium slab is also provided.

## Section S11: Free-electron Brewster-transition radiation from a gain slab with a fixed finite thickness

This section serves as the complementary information for Fig. 3. We show in Fig. S15 that for a gain slab with a fixed finite thickness, there would be an optimal non-zero value of $-Im(\varepsilon_{\text{r},2})$ to

achieve the free-electron Brewster-transition radiation with the strongest intensity (e.g. $-Im(\varepsilon_{r,2}) = 0.053$ for the case of $d/\lambda_0 = 40$).

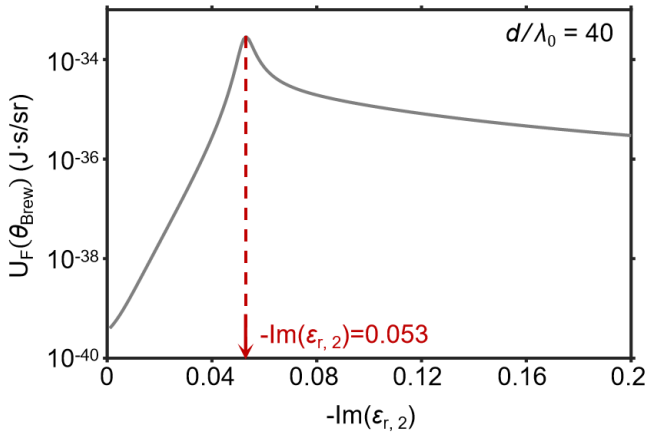


**Fig. S15. Forward angular energy density at the Brewster angle $U_F(\theta_{Brew})$ as a function of $-Im(\varepsilon_{r,2})$ when the gain slab has a fixed finite thickness $d$.** For illustration, here the gain slab has a finite thickness of $d/\lambda_0 = 40$. There is an optimal value of $-Im(\varepsilon_{r,2})$ to achieve the free-electron Brewster-transition radiation with the strongest intensity. For example, if $d/\lambda_0 = 40$, the free-electron Brewster-transition radiation with the strongest intensity appears at $-Im(\varepsilon_{r,2}) = 0.053$.

## Section S12: Free-electron Brewster-transition radiation from ultralow-energy electrons

This section serves as the complementary information for Fig. 4, and we show the forward angular spectral energy density $U_F(\theta_F)$ of free-electron radiation under the condition of $v/c = 10^{-5}$ in Fig. S16A and $10^{-7}$ in Fig. S16B.

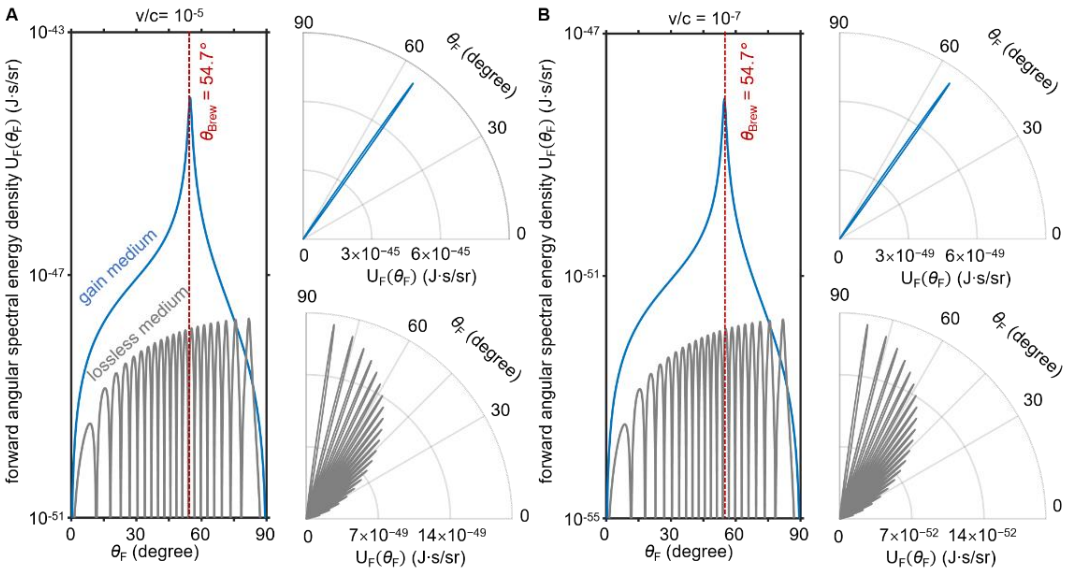


**Fig. S16 Forward angular spectral energy density $U_F(\theta_F)$ of free-electron radiation when the electron velocity is $v/c \ll 1$.** The structural setup here is the same as Fig. 1C, except for the electron velocity. For comparison, the forward angular spectral energy density of free-electron radiation from a transparent slab is also given. (**A**) The electron has a velocity of $v/c = 10^{-5}$. (**B**) The electron velocity is $v/c = 10^{-7}$.

## Section S13: Free-electron transition radiation from a Gaussian electron beam

In practice, an electron beam with a certain current density, instead of a single moving electron, would be applied for potential experimental demonstration. Once the current density of electron beam is low enough (e.g. in the order of nA or μA in scanning electron microscope (SEM) and transmission electron microscope (TEM)), the space charge and nonlinear effects are generally weak and can be neglected. Under this condition, the electromagnetic radiation from an electron beam can be readily considered as the interference of radiation from each moving electron. In other words, the model of single moving electron used in this work can well characterize the main feature of electromagnetic radiation from an electron beam. For example, if an electron beam with a relatively-

low current density and a Gaussian shape in $z$-direction is used, the induced current density $\bar{J}(\bar{r},t) = \hat{z}qv\delta(x)\delta(y)\delta(z-vt)$ in equation (S1) should be changed to $\bar{J}(\bar{r},t) = \hat{z}Nq\delta(x)\delta(y)\frac{1}{\sigma\sqrt{2\pi}}e^{-\frac{(z-vt)^2}{2\sigma^2}}$, where $\sigma$ is the standard deviation of Gaussian function and $N$ is the electron number. By applying the Fourier transformation, each Fourier component of the current density $j^q_{\bar{k}_\perp,\omega}(z) = \frac{q}{(2\pi)^3}e^{i\frac{\omega}{v}z}$ in equation (S5) should be changed to $j^q_{\bar{k}_\perp,\omega}(z) = \frac{Nqe^{-\frac{\sigma^2\omega^2}{2v^2}}}{(2\pi)^3}e^{i\frac{\omega}{v}z}$. Accordingly, the factor of $q$ in the expression of radiation field in equations (S10-S13) and the angular spectral energy density in equation (S42) should also be replaced with $Nqe^{-\frac{\sigma^2\omega^2}{2v^2}}$.

*Coherence of free-electron Brewster-transition radiation*

The revealed free-electron Brewster-transition radiation in this work results from the interference process of transition radiation induced by the electron's penetration through two parallel interfaces. This interference process directly reflects the coherent nature of free-electron Brewster-transition radiation, since the coherence is a necessary condition for interference. To be specific, we would like to point out that by following Ginzburg and Frank's theory of free-electron radiation, the moving electron is treated as a point source in the theoretical analysis, and its emitted waves are TM (i.e. *p*-polarized) waves when the electron perpendicularly crosses these interfaces. Then for a given frequency, the free-electron Brewster-transition radiation fulfills the interference conditions (i.e. same frequency, same polarization, and a constant phase difference between emitted waves at two points in space) and is thus essentially coherent.

In addition, we note that in practice, when considering the free-electron Brewster-transition radiation within a certain frequency range, instead of a given frequency, the corresponding temporal coherence would be sensitive to the frequency bandwidth. When considering the free-electron

Brewster-transition radiation from an electron beam, instead of a moving electron, the corresponding spatial coherence would be sensitive to the beam shape (e.g. the transverse beam size). Under these practical scenarios, the free-electron Brewster-transition radiation might become partially coherent or even incoherent.

**REFERENCE AND NOTES**


1. A. Fisher, Y. Park, M. Lenz, A. Ody, R. Agustsson, T. Hodgetts, A. Murokh, P. Musumeci, Single-pass high-efficiency terahertz free-electron laser. *Nat. Photon.* **16**, 441–447 (2022).

2. A. Konečná, F. Iyikanat, F. J. G. de Abajo, Entangling free electrons and optical excitations. *Sci. Adv.* **8**, eabo7853 (2022).

3. D. Zhang, Y. Zeng, Y. Bai, Z. Li, Y. Tian, R. Li, Coherent surface plasmon polariton amplification via free-electron pumping. *Nature* **611**, 55–60 (2022).

4. N. V. Sapra, K. Y. Yang, D. Vercruysse, K. J. Leedle, D. S. Black, R. J. England, L. Su, R. Trivedi, Y. Miao, O. Solgaard, R. L. Byer, J. Vučkovicć, On-chip integrated laser-driven particle accelerator. *Science* **367**, 79–83 (2020).

5. U. Bergmann, J. Kern, R. W. Schoenlein, P. Wernet, V. K. Yachandra, J. Yano, Using X-ray free-electron lasers for spectroscopy of molecular catalysts and metalloenzymes. *Nat. Rev. Phys.* **3**, 264–282 (2021).

6. N. Rivera, I. Kaminer, Light-matter interactions with photonic quasiparticles. *Nat. Rev. Phys.* **2**, 538–561 (2020).

7. H. Hu, X. Lin, Y. Luo, Free-electron radiation engineering via structured environments. *Prog. Electromagn. Res.* **171**, 75–88 (2021).

8. Z. Su, B. Xiong, Y. Xu, Z. Cai, J. Yin, R. Peng, Y. Liu, Manipulating Cherenkov radiation and Smith-Purcell radiation by artificial structures. *Adv. Opt. Mater.* **7**, 1801666 (2019).

9. W. Wang, K. Feng, L. Ke, C. Yu, Y. Xu, R. Qi, Y. Chen, Z. Qin, Z. Zhang, M. Fang, J. Liu, K. Jiang, H. Wang, C. Wang, X. Yang, F. Wu, Y. Leng, J. Liu, R. Li, Z. Xu, Free-electron lasing at 27 nanometres based on a laser wakefield accelerator. *Nature* **595**, 516–520 (2021).

10. W. Decking, S. Abeghyan, P. Abramian, A. Abramsky, A. Aguirre, C. Albrecht, P. Alou, M. Altarelli, P. Altmann, K. Amyan, V. Anashin, E. Apostolov, K. Appel, D. Auguste, V. Ayvazyan, S. Baark, F. Babies, N. Baboi, P. Bak, V. Balandin, R. Baldinger, B. Baranasic, S.

Barbanotti, O. Belikov, V. Belokurov, L. Belova, V. Belyakov, S. Berry, M. Bertucci, B. Beutner, A. Block, M. Blöcher, T. Böckmann, C. Bohm, M. Böhnert, V. Bondar, E. Bondarchuk, M. Bonezzi, P. Borowiec, C. Bösch, U. Bösenberg, A. Bosotti, R. Böspflug, M. Bousonville, E. Boyd, Y. Bozhko, A. Brand, J. Branlard, S. Briechle, F. Brinker, S. Brinker, R. Brinkmann, S. Brockhauser, O. Brovko, H. Brück, A. Brüdgam, L. Butkowski, T. Büttner, J. Calero, E. Castro-Carballo, G. Cattalanotto, J. Charrier, J. Chen, A. Cherepenko, V. Cheskidov, M. Chiodini, A. Chong, S. Choroba, M. Chorowski, D. Churanov, W. Cichalewski, M. Clausen, W. Clement, C. Cloué, J. A. Cobos, N. Coppola, S. Cunis, K. Czuba, M. Czwalinna, B. D'Almagne, J. Dammann, H. Danared, A. de Zubiaurre Wagner, A. Delfs, T. Delfs, F. Dietrich, T. Dietrich, M. Dohlus, M. Dommach, A. Donat, X. Dong, N. Doynikov, M. Dressel, M. Duda, P. Duda, H. Eckoldt, W. Ehsan, J. Eidam, F. Eints, C. Engling, U. Englisch, A. Ermakov, K. Escherich, J. Eschke, E. Saldin, M. Faesing, A. Fallou, M. Felber, M. Fenner, B. Fernandes, J. M. Fernández, S. Feuker, K. Filippakopoulos, K. Floettmann, V. Fogel, M. Fontaine, A. Francés, I. F. Martin, W. Freund, T. Freyermuth, M. Friedland, L. Fröhlich, M. Fusetti, J. Fydrych, A. Gallas, O. García, L. Garcia-Tabares, G. Geloni, N. Gerasimova, C. Gerth, P. Geßler, V. Gharibyan, M. Gloor, J. Głowinkowski, A. Goessel, Z. Gołębiewski, N. Golubeva, W. Grabowski, W. Graeff, A. Grebentsov, M. Grecki, T. Grevsmuehl, M. Gross, U. Grosse-Wortmann, J. Grünert, S. Grunewald, P. Grzegory, G. Feng, H. Guler, G. Gusev, J. L. Gutierrez, L. Hagge, M. Hamberg, R. Hanneken, E. Harms, I. Hartl, A. Hauberg, S. Hauf, J. Hauschildt, J. Hauser, J. Havlicek, A. Hedqvist, N. Heidbrook, F. Hellberg, D. Henning, O. Hensler, T. Hermann, A. Hidvégi, M. Hierholzer, H. Hintz, F. Hoffmann, M. Hoffmann, M. Hoffmann, Y. Holler, M. Hüning, A. Ignatenko, M. Ilchen, A. Iluk, J. Iversen, J. Iversen, M. Izquierdo, L. Jachmann, N. Jardon, U. Jastrow, K. Jensch, J. Jensen, M. Jeżabek, M. Jidda, H. Jin, N. Johansson, R. Jonas, W. Kaabi, D. Kaefer, R. Kammering, H. Kapitza, S. Karabekyan, S. Karstensen, K. Kasprzak, V. Katalev, D. Keese, B. Keil, M. Kholopov, M. Killenberger, B. Kitaev, Y. Klimchenko, R. Klos, L. Knebel, A. Koch, M. Koepke, S. Köhler, W. Köhler, N. Kohlstrunk, Z. Konopkova, A. Konstantinov, W. Kook, W. Koprek, M. Körfer, O. Korth, A. Kosarev, K. Kosiński, D. Kostin, Y. Kot, A. Kotarba, T. Kozak, V. Kozak, R. Kramert, M. Krasilnikov, A. Krasnov, B. Krause, L. Kravchuk, O. Krebs, R. Kretschmer, J. Kreutzkamp, O. Kröplin, K. Krzysik, G. Kube, H. Kuehn, N. Kujala, V. Kulikov, V. Kuzminych, D. La Civita, M. Lacroix, T. Lamb, A.

Lancetov, M. Larsson, D. Le Pinvidic, S. Lederer, T. Lensch, D. Lenz, A. Leuschner, F. Levenhagen, Y. Li, J. Liebing, L. Lilje, T. Limberg, D. Lipka, B. List, J. Liu, S. Liu, B. Lorbeer, J. Lorkiewicz, H. H. Lu, F. Ludwig, K. Machau, W. Maciocha, C. Madec, C. Magueur, C. Maiano, I. Maksimova, K. Malcher, T. Maltezopoulos, E. Mamoshkina, B. Manschwetus, F. Marcellini, G. Marinkovic, T. Martinez, H. Martirosyan, W. Maschmann, M. Maslov, A. Matheisen, U. Mavric, J. Meißner, K. Meissner, M. Messerschmidt, N. Meyners, G. Michalski, P. Michelato, N. Mildner, M. Moe, F. Moglia, C. Mohr, S. Mohr, W. Möller, M. Mommerz, L. Monaco, C. Montiel, M. Moretti, I. Morozov, P. Morozov, D. Mross, J. Mueller, C. Müller, J. Müller, K. Müller, J. Munilla, A. Münnich, V. Muratov, O. Napoly, B. Näser, N. Nefedov, R. Neumann, R. Neumann, N. Ngada, D. Noelle, F. Obier, I. Okunev, J. A. Oliver, M. Omet, A. Oppelt, A. Ottmar, M. Oublaid, C. Pagani, R. Paparella, V. Paramonov, C. Peitzmann, J. Penning, A. Perus, F. Peters, B. Petersen, A. Petrov, I. Petrov, S. Pfeiffer, J. Pflüger, S. Philipp, Y. Pienaud, P. Pierini, S. Pivovarov, M. Planas, E. Pławski, M. Pohl, J. Polinski, V. Popov, S. Prat, J. Prenting, G. Priebe, H. Pryschelski, K. Przygoda, E. Pyata, B. Racky, A. Rathjen, W. Ratuschni, S. Regnaud-Campderros, K. Rehlich, D. Reschke, C. Robson, J. Roever, M. Roggli, J. Rothenburg, E. Rusiński, R. Rybaniec, H. Sahling, M. Salmani, L. Samoylova, D. Sanzone, F. Saretzki, O. Sawlanski, J. Schaffran, H. Schlarb, M. Schlösser, V. Schlott, C. Schmidt, F. Schmidt-Foehre, M. Schmitz, M. Schmökel, T. Schnautz, E. Schneidmiller, M. Scholz, B. Schöneburg, J. Schultze, C. Schulz, A. Schwarz, J. Sekutowicz, D. Sellmann, E. Semenov, S. Serkez, D. Sertore, N. Shehzad, P. Shemarykin, L. Shi, M. Sienkiewicz, D. Sikora, M. Sikorski, A. Silenzi, C. Simon, W. Singer, X. Singer, H. Sinn, K. Sinram, N. Skvorodnev, P. Smirnow, T. Sommer, A. Sorokin, M. Stadler, M. Steckel, B. Steffen, N. Steinhau-Kühl, F. Stephan, M. Stodulski, M. Stolper, A. Sulimov, R. Susen, J. Świerblewski, C. Sydlo, E. Syresin, V. Sytchev, J. Szuba, N. Tesch, J. Thie, A. Thiebault, K. Tiedtke, D. Tischhauser, J. Tolkiehn, S. Tomin, F. Tonisch, F. Toral, I. Torbin, A. Trapp, D. Treyer, G. Trowitzsch, T. Trublet, T. Tschentscher, F. Ullrich, M. Vannoni, P. Varela, G. Varghese, G. Vashchenko, M. Vasic, C. Vazquez-Velez, A. Verguet, S. Vilcins-Czvitkovits, R. Villanueva, B. Visentin, M. Viti, E. Vogel, E. Volobuev, R. Wagner, N. Walker, T. Wamsat, H. Weddig, G. Weichert, H. Weise, R. Wenndorf, M. Werner, R. Wichmann, C. Wiebers, M. Wiencek, T. Wilksen, I. Will, L. Winkelmann, M. Winkowski, K. Wittenburg, A. Witzig, P. Wlk, T. Wohlenberg, M. Wojciechowski, F. Wolff-Fabris, G.

Wrochna, K. Wrona, M. Yakopov, B. Yang, F. Yang, M. Yurkov, I. Zagorodnov, P. Zalden, A. Zavadtsev, D. Zavadtsev, A. Zhirnov, A. Zhukov, V. Ziemann, A. Zolotov, N. Zolotukhina, F. Zummack, D. Zybin, A MHz-repetition-rate hard X-ray free-electron laser driven by a superconducting linear accelerator. *Nat. Photon.* **14**, 391–397 (2020).

11. B. McNeil, N. Thompson, X-ray free-electron lasers. *Nat. Photon.* **4**, 814–821 (2010).

12. E. Prat, R. Abela, M. Aiba, A. Alarcon, J. Alex, Y. Arbelo, C. Arrell, V. Arsov, C. Bacellar, C. Beard, P. Beaud, S. Bettoni, R. Biffiger, M. Bopp, H.-H. Braun, M. Calvi, A. Cassar, T. Celcer, M. Chergui, P. Chevtsov, C. Cirelli, A. Citterio, P. Craievich, M. C. Divall, A. Dax, M. Dehler, Y. Deng, A. Dietrich, P. Dijkstal, R. Dinapoli, S. Dordevic, S. Ebner, D. Engeler, C. Erny, V. Esposito, E. Ferrari, U. Flechsig, R. Follath, F. Frei, R. Ganter, T. Garvey, Z. Geng, A. Gobbo, C. Gough, A. Hauff, C. P. Hauri, N. Hiller, S. Hunziker, M. Huppert, G. Ingold, R. Ischebeck, M. Janousch, P. J. M. Johnson, S. L. Johnson, P. Juranić, M. Jurcevic, M. Kaiser, R. Kalt, B. Keil, D. Kiselev, C. Kittel, G. Knopp, W. Koprek, M. Laznovsky, H. T. Lemke, D. L. Sancho, F. Löhl, A. Malyzhenkov, G. F. Mancini, R. Mankowsky, F. Marcellini, G. Marinkovic, I. Martiel, F. Märki, C. J. Milne, A. Mozzanica, K. Nass, G. L. Orlandi, C. O. Loch, M. Paraliev, B. Patterson, L. Patthey, B. Pedrini, M. Pedrozzi, C. Pradervand, P. Radi, J.-Y. Raguin, S. Redford, J. Rehanek, S. Reiche, L. Rivkin, A. Romann, L. Sala, M. Sander, T. Schietinger, T. Schilcher, V. Schlott, T. Schmidt, M. Seidel, M. Stadler, L. Stingelin, C. Svetina, D. M. Treyer, A. Trisorio, C. Vicario, D. Voulot, A. Wrulich, S. Zerdane, E. Zimoch, A compact and cost-effective hard x-ray free-electron laser driven by a high-brightness and low-energy electron beam. *Nat. Photon.* **14**, 748–754 (2020).

13. A. K. Kaminsky, É. A. Perel'shteĭn, S. N. Sedykh, N. S. Ginzburg, S. V. Kuzikov, N. Y. Peskov, A. S. Sergeev, Demonstrating high-power 30-GHz free-electron maser operation on a resonant load. *Tech. Phys. Lett.* **36**, 211–215 (2010).

14. J. Gardelle, J. Labrouche, J. L. Rullier, Direct observation of beam bunching produced by a high power microwave free-electron laser. *Phys. Rev. Lett.* **76**, 4532–4535 (1996).

15. O. Chamberlain, E. Segrè, C. Wiegand, T. Ypsilantis, Observation of antiprotons. *Phys. Rev.* **100**, 947–950 (1955).

16. J. J. Aubert, U. Becker, P. J. Biggs, J. Burger, M. Chen, G. Everhart, P. Goldhagen, J. Leong, T. Mc Corriston, T. G. Rhoades, M. Rohde, S. C. C. Ting, S. L. Wu, Y. Y. Lee, Experimental observation of a heavy particle *J*. *Phys. Rev. Lett.* **33**, 1404–1406 (1974).

17. W. Galbraith, J. V. Jelley, Light pulses from the night sky associated with cosmic rays. *Nature* **171**, 349–350 (1953).

18. X. Lin, S. Easo, Y. Shen, H. Chen, B. Zhang, J. D. Joannopoulos, M. Soljačić, I. Kaminer, Controlling Cherenkov angles with resonance transition radiation. *Nat. Phys.* **14**, 816–821 (2018).

19. X. Lin, H. Hu, S. Easo, Y. Yang, Y. Shen, K. Yin, M. P. Blago, I. Kaminer, B. Zhang, H. Chen, J. Joannopoulos, M. Soljačić, Y. Luo, A Brewster route to Cherenkov detectors. *Nat. Commun.* **12**, 5554 (2021).

20. I. Nozawa, K. Kan, J. Yang, A. Ogata, T. Kondoh, M. Gohdo, K. Norizawa, H. Kobayashi, H. Shibata, S. Gonda, Y. Yoshida, Measurement of $< 20$ fs bunch length using coherent transition radiation. *Phys. Rev. ST Accel. Beams* **17**, 072803 (2014).

21. A. H. Lumpkin, R. Dejus, W. J. Berg, M. Borland, Y. C. Chae, E. Moog, N. S. Sereno, B. X. Yang, First observation of $z$-dependent electron-beam microbunching using coherent transition radiation. *Phys. Rev. Lett.* **86**, 79–82 (2001).

22. F. J. G. de Abajo, Optical excitations in electron microscopy. *Rev. Mod. Phys.* **82**, 209–275 (2010).

23. T. Shaffer, E. Pratt, J. Grimm, Utilizing the power of Cerenkov light with nanotechnology. *Nat. Nanotech.* **12**, 106–117 (2017).

24. Y. Yang, C. Roques-Carmes, S. E. Kooi, H. Tang, J. Beroz, E. Mazur, I. Kaminer, J. D. Joannopoulos, M. Soljačić, Photonic flatband resonances for free-electron radiation. *Nature* **613**, 42–47 (2023).

25. R. Dahan, S. Nehemia, M. Shentcis, O. Reinhardt, Y. Adiv, X. Shi, O. Be'er, M. H. Lynch, Y. Kurman, K. Wang, I. Kaminer, Resonant phase-matching between a light wave and a free-electron wavefunction. *Nat. Phys.* **16**, 1123–1131 (2020).

26. R. Dahan, G. Baranes, A. Gorlach, R. Ruimy, N. Rivera, I. Kaminer, Creation of optical cat and GKP states using shaped free electrons. arXiv:2206.08828 [quant-ph] (2022); https://doi.org/10.48550/arXiv.2206.08828.

27. G. Baranes, R. Ruimy, A. Gorlach, I. Kaminer, Free electrons can induce entanglement between photons. *npj Quantum Inf.* **8**, 32 (2022).

28. S. Huang, R. Duan, N. Pramanik, C. Boothroyd, Z. Liu, L. J. Wong, Enhanced versatility of table-top x-rays from Van der Waals structures. *Adv. Sci.* **9**, 2105401 (2022).

29. S. Huang, R. Duan, N. Pramanik, J. S. Herrin, C. Boothroyd, Z. Liu, L. J. Wong, Quantum recoil in free-electron interactions with atomic lattices. *Nat. Photon.* **17**, 224–230 (2023).

30. L. J. Wong, I. Kaminer, Prospects in x-ray science emerging from quantum optics and nanomaterials. *Appl. Phys. Lett.* **119**, 130502 (2021).

31. F. J. G. de Abajo, V. Di Giulio, Optical excitations with electron beams: Challenges and opportunities. *ACS Photonics* **8**, 945–974 (2021).

32. C. Roques-Carmes, S. E. Kooi, Y. Yang, N. Rivera, P. D. Keathley, J. D. Joannopoulos, S. G. Johnson, I. Kaminer, K. K. Berggren, M. Soljačić, Free-electron-light interactions in nanophotonics. *Appl. Phys. Rev.* **10**, 011303 (2023).

33. J. J. M. Madey, Stimulated emission of bremsstrahlung in a periodic magnetic field. *J. Appl. Phys.* **42**, 1906–1913 (1971).

34. J. Duris, S. Li, T. Driver, E. G. Champenois, J. P. MacArthur, A. A. Lutman, Z. Zhang, P. Rosenberger, J. W. Aldrich, R. Coffee, G. Coslovich, F.-J. Decker, J. M. Glownia, G. Hartmann, W. Helml, A. Kamalov, J. Knurr, J. Krzywinski, M.-F. Lin, J. P. Marangos, M. Nantel, A. Natan, J. T. O'Neal, N. Shivaram, P. Walter, A. L. Wang, J. J. Welch, T. J. A. Wolf,

J. Z. Xu, M. F. Kling, P. H. Bucksbaum, A. Zholents, Z. Huang, J. P. Cryan, A. Marinelli, Tunable isolated attosecond x-ray pulses with gigawatt peak power from a free-electron laser. *Nat. Photon.* **14**, 30–36 (2020).

35. A. F. Habib, G. G. Manahan, P. Scherkl, T. Heinemann, A. Sutherland, R. Altuiri, B. M. Alotaibi, M. Litos, J. Cary, T. Raubenheimer, E. Hemsing, M. J. Hogan, J. B. Rosenzweig, P. H. Williams, B. W. J. McNeil, B. Hidding, Attosecond-angstrom free-electron-laser towards the cold beam limit. *Nat. Commun.* **14**, 1054 (2023).

36. Cherenkov, P. A. Radiation from high-speed particles. *Science* **131**, 136–142 (1960).

37. Frank, I. M. Optics of light sources moving in refractive media. *Science* **131**, 702–712 (1960).

38. R. Shiloh, N. Schönenberger, Y. Adiv, R. Ruimy, A. Karnieli, T. Hughes, R. J. England, K. J. Leedle, D. S. Black, Z. Zhao, P. Musumeci, R. L. Byer, A. Arie, I. Kaminer, P. Hommelhoff, Miniature light-driven nanophotonic electron acceleration and control. *Adv. Opt. Photonics* **14**, 862–932 (2022).

39. C. Roques-Carmes, S. E. Kooi, Y. Yang, A. Massuda, P. D. Keathley, A. Zaidi, Y. Yang, J. D. Joannopoulos, K. K. Berggren, I. Kaminer, M. Soljačić, Towards integrated tunable all-silicon free-electron light sources. *Nat. Commun.* **10**, 3176 (2019).

40. H. Hu, X. Lin, L. J. Wong, Q. Yang, B. Zhang, Y. Luo, Surface Dyakonov–Cherenkov radiation. *eLight* **2**, 2 (2022).

41. I. P. Ivanov, D. V. Karlovets, Detecting transition radiation from a magnetic moment. *Phys. Rev. Lett.* **110**, 264801 (2013).

42. H. Hu, X. Lin, D. Liu, H. Chen, B. Zhang, Y. Luo, Broadband enhancement of Cherenkov radiation using dispersionless plasmons. *Adv. Sci.* **9**, 2200538 (2022).

43. X. Xu, D. B. Cesar, S. Corde, V. Yakimenko, M. J. Hogan, C. Joshi, A. Marinelli, W. B. Mori, Generation of terawatt attosecond pulses from relativistic transition radiation. *Phys. Rev. Lett.* **126**, 094801 (2021).

44. M. Shentcis, A. K. Budniak, X. Shi, R. Dahan, Y. Kurman, M. Kalina, H. H. Sheinfux, M. Blei, M. K. Svendsen, Y. Amouyal, S. Tongay, K. S. Thygesen, F. H. L. Koppens, E. Lifshitz, F. J. G. de Abajo, L. J. Wong, I. Kaminer, Tunable free-electron x-ray radiation from van der Waals materials. *Nat. Photon.* **14**, 686–692 (2020).

45. F. Liu, L. Xiao, Y. Ye, M. Wang, K. Cui, X. Feng, W. Zhang, Y. Huang, Integrated Cherenkov radiation emitter eliminating the electron velocity threshold. *Nat. Photon.* **11**, 289–292 (2017).

46. X. Lin, I. Kaminer, X. Shi, F. Gao, Z. Yang, Z. Gao, H. Buljan, J. D. Joannopoulos, M. Soljačić, H. Chen, B. Zhang, Splashing transients of 2D plasmons launched by swift electrons. *Sci. Adv.* **3**, e1601192 (2017).

47. Z. Duan, X. Tang, Z. Wang, Y. Zhang, X. Chen, M. Chen, Y. Gong, Observation of the reversed Cherenkov radiation. *Nat. Commun.* **8**, 14901 (2017).

48. L. J. Wong, I. Kaminer, O. Ilic, J. D. Joannopoulos, M. Soljačić, Towards graphene plasmon-based free-electron infrared to x-ray sources. *Nat. Photon.* **10**, 46–52 (2016).

49. P. Genevet, D. Wintz, A. Ambrosio, A. She, R. Blanchard, F. Capasso, Controlled steering of Cherenkov surface plasmon wakes with a one-dimensional metamaterial. *Nat. Nanotech.* **10**, 804–809 (2015).

50. S. Liu, P. Zhang, W. Liu, S. Gong, R. Zhong, Y. Zhang, M. Hu, Surface polariton Cherenkov light radiation source. *Phys. Rev. Lett.* **109**, 153902 (2012).

51. F. Tay, X. Lin, X. Shi, H. Chen, I. Kaminer, B. Zhang, Bulk-plasmon-mediated free-electron radiation beyond the conventional formation time. *Adv. Sci.*, 2300760 (2023).

52. A. A. Kolokolov **2023**, Reflection of plane-waves from an amplifying medium. *ZhETF Pis. Red.* **21**, 312–313 (1975).

53. X. Lin, Y. Shen, I. Kaminer, H. Chen, M. Soljačić, Transverse-electric Brewster effect enabled by nonmagnetic two-dimensional materials. *Phys. Rev. A* **94**, 023836 (2016).

54. A. V. Dorofeenko, A A Zyablovsky, A. A. Pukhov, A A Lisyansky, A. P. Vinogradov, Light propagation in composite materials with gain layers. *Physics-Uspekhi* **55**, 1080–1097 (2012).

55. L.-G. Wang, L. Wang, M. Al-Amri, S.-Y. Zhu, M. Suhail Zubairy, Counterintuitive dispersion violating Kramers-Kronig relations in gain slabs. *Phys. Rev. Lett.* **112**, 233601 (2014).

56. S. Y. Kim, K. Vedam, Analytic solution of the pseudo-Brewster angle. *J. Opt. Soc. Am. A* **3**, 1772–1773 (1986).

57. A. Lakhtakia, Would Brewster recognize today's Brewster angle? *Optics News* **15**, 14–18 (1989).

58. H. Fan, H. Chu, H. Luo, Y. Lai, L. Gao, J. Luo, Brewster metasurfaces for ultrabroadband reflectionless absorption at grazing incidence. *Optica* **9**, 1138–1148 (2022).

59. J. Luo, H. Chu, R. Peng, M. Wang, J. Li, Y. Lai, Ultra-broadband reflectionless Brewster absorber protected by reciprocity. *Light Sci. Appl.* **10**, 89 (2021).

60. V. L. Ginzburg, Radiation of a uniformly moving electron due to its transition from one medium into another. *Sov. Phys. JETP* **16**, 15–28 (1946).

61. V. L. Ginzburg, V. N. Tsytovich, *Transition Radiation and Transition Scattering* (CRC Press, 1990).

62. J. Chen, R. Chen, Z. Gong, H. Hu, Y. Yang, X. Zhang, C. Wang, I. Kaminer, H. Chen, B. Zhang, X. Lin, Low-velocity-favored transition radiation. arXiv:2212.13066 [physics.optics] (2022); https://doi.org/10.48550/arXiv.2212.13066.

63. R. Chen, Z. Gong, J. Chen, X. Zhang, X. Zhu, H. Chen, X. Lin, Recent advances of transition radiation: Fundamentals and applications. *Mater. Today Electron.* **3**, 100025 (2023).

64. G. M. Garibyan, Transition radiation effects in particle energy losses. *Soviet Physics JETP* **37,** 527–533 (1959).

65. C. Qian, Y. Yang, Y. Hua, C. Wang, X. Lin, T. Cai, D. Ye, E. Li, I. Kaminer, H. Chen, Breaking the fundamental scattering limit with gain metasurfaces. *Nat. Commun.* **13**, 4383 (2022).

66. D. Ye, K. Chang, L. Ran, H. Xin, Microwave gain medium with negative refractive index. *Nat. Commun.* **5**, 5841 (2014).

67. W. Xu, W. J. Padilla, S. Sonkusale, Loss compensation in metamaterials through embedding of active transistor based negative differential resistance circuits. *Opt. Express* **20,** 22406–22411 (2012).

68. T. Jiang, K. Chang, L.-M. Si, L. Ran, H. Xin, Active microwave negative-index metamaterial transmission line with gain. *Phys. Rev. Lett.* **107**, 205503 (2011).

69. I. de Leon, P. Berini, Amplification of long-range surface plasmons by a dipolar gain medium. *Nat. Photon.* **4**, 382–387 (2010).

70. M. C. Gather, K. Meerholz, N. Danz, K. Leosson, Net optical gain in a plasmonic waveguide embedded in a fluorescent polymer. *Nat. Photon.* **4**, 457–461 (2010).

71. A. Fang, T. Koschny, C. M. Soukoulis, Lasing in metamaterial nanostructures. *J. Opt.* **12**, 024013 (2010).

72. J. E. Geusic, H. M. Marcos, L. Van Uitert, Laser oscillations in Nd-doped yttrium aluminum, yttrium gallium and gadolinium garnets. *Appl. Phys. Lett.* **4**, 182–184 (1964).

73. F. Hide, M. A. Díaz-García, B. J. Schwartz, M. R. Andersson, Q. Pei, A. J. Heeger, Semiconducting polymers: A new class of solid-state laser materials. *Science* **273**, 1833–1836 (1996).

74. G. Adamo, K. F. MacDonald, Y. H. Fu, C.-M. Wang, D. P. Tsai, F. J. G. de Abajo, N. I. Zheludev, Light well: A tunable free-electron light source on a chip. *Phys. Rev. Lett.* **103**, 113901 (2009).

75. Z. Dang, Y. Huang, Z. Liu, L. Zheng, X. He, Z. Liu, Y. Dai, Z. Fang, Chiral Smith-Purcell radiation light source. *Adv. Opt. Mater.*, 2300274 (2023).

76. J. Chen, H. Chen, X. Lin, Photonic and plasmonic transition radiation from graphene. *J. Opt.* **23**, 034001 (2021).

77. J. A. Kong, *Electromagnetic Wave Theory* (EMW Publishing, 2008).

78. D. Brewster, On the laws which regulate the polarization of light by reflection from transparent bodies. *Proc. R. Soc. Lond. Series* **2**, 14–15 (1815).

79. R. Paniagua-Domínguez, Y. F. Yu, A. E. Miroshnichenko, L. A. Krivitsky, Y. H. Fu, V. Valuckas, L. Gonzaga, Y. T. Toh, A. Y. S. Kay, B. Luk'yanchuk, A. I. Kuznetsov, Generalized Brewster effect in dielectric metasurfaces. *Nat. Commun.* **7**, 10362 (2016).

80. Y. Shen, D. Ye, I. Celanovic, S. G. Johnson, J. D. Joannopoulos, M. Soljačić, Optical broadband angular selectivity. *Science* **343**, 1499–1501 (2014).

81. M. A. Noginov, V. A. Podolskiy, G. Zhu, M. Mayy, M. Bahoura, J. A. Adegoke, B. A. Ritzo, K. Reynolds, Compensation of loss in propagating surface plasmon polariton by gain in adjacent dielectric medium. *Opt. Express* **16**, 1385–1392 (2008).